# THREE PHASE BRUSHLESS DC MOTOR

# ANALYSIS AND DRIVE CIRCUIT DESIGN

**A Thesis Submitted to the**

**Graduate School of Natural and Applied Sciences of**

**Dokuz Eylül University**

**In Partial Fulfillment of the Requirements for**

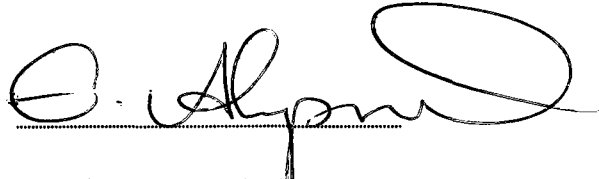**the Degree of Master of Science in Electrical and Electronics Engineering**

*136781*

**by**
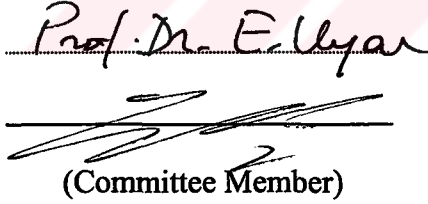
**Cenk CENGİZ**

**January, 2003**
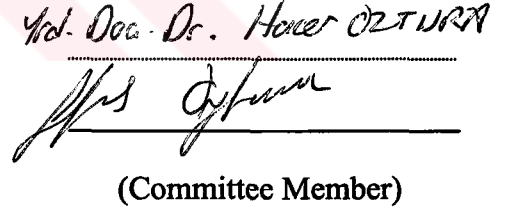
**İZMİR**

# M.Sc THESIS EXAMINATION RESULT FORM

We certify that we have read this thesis and **"THREE PHASE BRUHSLESS DC MOTOR ANALYSIS AND DRIVE CIRCUIT DESIGN"** completed by **Cenk CENGİZ** under supervision of **Prof. Dr Eyüp AKPINAR** and that in our opinion it is fully adequate, in scope and in quality, as a thesis for the degree of Master of Science.
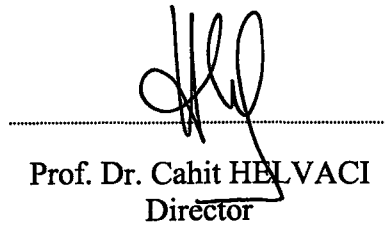
Prof. Dr. Eyüp AKPINAR

Supervisor

(Committee Member)

(Committee Member)

Approved by the

Graduate School of Natural and Applied Sciences

Prof. Dr. Cahit HELVACI

Director

# ACKNOWLEDGEMENTS

I would like to thank my supervisor Prof. Dr. Eyüp AKPINAR for his valuable guidance and support during the course of this thesis. I wish to express my sincere appreciation to Rsrch. Asst. Tolga SÜRGEVİL for his helpful advice and Osman GERGÖZ from Faz Elektrik for his support. Finally, 1 thank my parents and my friend Ekin SERTOĞLU for their understanding and never ending support throughout my life.

Cenk CENGİZ

# ABSTRACT

In this thesis, to analyze brushless DC (BLDC) motor, a computer simulation program and an implemented circuit are used and the results are compared.

Features, structures, torque profile and torque/speed characteristics of BLDC motor are explained, then the mathematical model motor are obtained. Motor parameters are measured, which are necessary for simulation program.

In simulation program, 3-phase six-step bridge inverter having 6 MOSFETs has fed the BLDC motor at 120-degree conduction mode. By using the direct back emf detection the correct commutation sequence is selected.

In implemented circuit, 8 poles BLDC motor is connected TDA5142T Brushless DC Motor Drive Circuit of Philips. The BLDC motor has been fed by 3-phase six-step bridge inverter having 6 MOSFETs. Sensorless control is used. Back emf comparator detects the zero crossings in the motor back emf and they are used to calculate the correct moment for the next commutation.

Closed loop control is applied to the computer simulation program. For the speed control, PI controller is used. The coefficients of PI controller are determined. The PWM is only applied to the high side MOSFETs for the detection of the zero crossing events. The control principal of simulation is to obtain maximum efficiency from the motor by keeping the phase current in phase with the back emf in the same winding. The phase current is limited to 20 A at the starting.

**Keywords:** Brushless DC motor, sensorless control, closed loop control

# ÖZET

Bu tezde fırçasız doğru akım motoru analiz edilmiştir. Bu amaçla bilgisayar ortamında simulasyon ve laboratuvar ortamında deneysel çalışmalar yapılmıştır, ve bunların sonuçları karşılaştırılmıştır.

Fırçasız doğru akım motorunun özellikleri, yapısı, tork profili ve tork/hız karekteristiği anlatılmış, daha sonrada motorun matematiksel modeli elde edilmiştir. Matlab Simulink, simulasyon programında gerekli olan bazı motor parametreleri hesaplanmıştır. Simulasyon programında 6 tane MOSFET'li üç faz tam köprü invertör modeli, 120 derece iletim modunda fırçasız doğru akım motoru modelini besler. Direk olarak emk'yı (emf) algılıyarak, doğru iletim sırası seçilir.

Laboratuvar ortamında, 8 kutuplu fırçasız doğru akım motoru, 6 tane MOSFET'li üç faz tam köprü invertöre bağlanır. Bu invertörün iletim sırasını, özel olarak fırçasız doğru akım motorları için üretilmiş Philips'in TDA5142T numaralı sürücü entegresi belirler. Bu entegrede sensörsüz kontrol kullanılır. TDA5142T'deki Emf karşılaştırıcısı, emfdeki sıfır geçişlerini algılıyarak, doğru iletimi sağlar

Simulasyon programında kapalı çevirim kontrolüde uygulanmıştır. Hız kontrolü için PI kontrol yöntemi uygulanmıştır, bunun için gerekli olan PI parametreleri hesaplanmıştır. PWM sadece üstteki MOSFET'lere uygulanmıştır. Simulasyonun kontrol prensibi, motordan maximum enerji elde etmek için, motorun faz akımı ile o fazın emf'sinin aynı fazda olmasıdır. Ayrıca başlangıçta motorun faz akımları 20 amper'de sınırlanmıştır.

**Anahtar sözcükler:** Fırçasız doğru akım motoru, sensörsüz kontrol, kapalı çevirim kontrolü.

# CONTENTS

**Chapter One**

**INTRODUCTION**

**Chapter Two**

**BRUSHLESS DC MOTOR**

**Chapter Three**

**BRUSHLESS DC MOTOR MODELLING**

**Chapter Four**

**BRUSHLESS DC MOTOR DRIVE CIRCUIT TDA5142T**

## Chapter Five
## SIMULATION RESULTS AND EXPERIMENTAL RESULTS

## Chapter Six
## CONCLUSIONS

# LIST OF TABLES

# LIST OF FIGURES

# CHAPTER ONE

# INTRODUCTION

A large fraction of electrical energy consumed in many facilities is used to run electric motors. Nationally, motor driven systems account for about 60 % of all electrical energy use (Bose, B.K., 1989).

Electrical motors are used in many industrial applications. These motors range from small "servo" motors to large motors used to lift thousands pounds. Each electric motor converts electrical energy to mechanical energy. Motors are selected for each application based on the amount of mechanical power. However, mechanical power is not the only criteria for choosing a motor. Different types of motors have different characteristics such as how much starting torque they provide, whether they operate at one speed or variable speeds and how efficient they are, etc.

Choosing the correct types of motors to use and properly maintaining them essential steps in the process of creating an efficient, cost-effective and failure-free production environment. The process can be greatly simplified and accelerated if an appropriate computer simulation tool is available.

Electric motors are the heart of today's industry, therefore over than 5 billion motors are built worldwide every year. In the last years the industrial appliance market is becoming a strong competitive field. The growing performances/costs ratio is leading the industry to new approaches in the motor control field in order to satisfy EMI/EMC laws, quality and reliability standards, etc.

The results of these constraining factors are long life motors, maintenance-free motors and sensor removal requirements, high efficiency driving and so on.

Brushless DC (BLDC) motor satisfies the above requirements. BLDC motor is a basically a permanent magnet synchronous motor which currently plays an increasing role in many industrial applications due to the following reasons.

- High power mass ratio
- Good heat dissipation characteristics
- Low rotor inertia
- High-speed capabilities (Subaşı, Y., 1998).

Moreover, when the application does not require high dynamic performances in the handling of the load torque, a sensorless control of the BLDC motor is a suitable low-cost implementation.

Adjustable speed drives for industrial appliance systems, large fans, compressors, hydraulic pumps, etc are good examples of system in which the load does not change suddenly and then a sensorless approach could be enough, as in this study.

The earliest evidence of a BLDC motor was in 1962 when T. G. Wilson and P. H. Trickey made a "DC Machine with Solid State Commutation". Unfortunately, the technology to make such a motor practical for industrial use over 5 hp simply did not exist until a number of years later. With the advent of powerful and permanent magnet materials and high power, high voltage transistors in the early to mid 80's the ability to make such a motor practical become a reality (Lee, E.C.).

Although BLDC motor has superior features such as high efficiency, greatly reduced maintenance, high reliability, elimination of brush debris, low acoustical and electrical noise, small size and a large speed range, designers are still reluctant to specify brushless motors because of concerns about cost. However, the cost of using BLDC motors have been falling over the past few years so that in many applications,

they can compete on cost alone. This is due to three major factors: advances in magnet technology, improvements in motor control electronics, and capital investments by BLDC motor manufacturers. As a result, BLDC motors are being used in a wide range cost sensitive applications including automotive, printers, plotters, computer peripherals, document sorters, and sewing machines.

BLDC motors are similar to brush PM motors. However, electronic commutation eliminates the brushes and the mechanical commutator. Commutators are subject to fairly restrictive limits on peripheral speed, voltage between segments, and current density. The maximum speed of the brushless motor is limited by the retention of the magnets against centrifugal force. In small motors with low rotor speeds, the magnets may be bonded to the rotor core, which is usually solid. The bonding must obviously have a wide temperature range and good ageing properties. For high rotor peripheral speeds it is necessary to provide a retaining structure such as a stainless-steel can or a kevlar or wire wrap. This may necessitate an increase in the mechanical airgap, but fortunately the performance is unduly sensitive to the airgap, which is often twice as large as in induction motors or switched reluctance motors (Miller, T.J.E., 1989). BLDC motors have many advantages, most of which listed in Table 1.1.

**Table 1.1 Brushless motor features**

| BLDC Advantage | Why BLDC provides this advantage. |
|---|---|
| Improved efficiency | Eliminate brush voltage drop and brush-friction. |
| Reduced electrical noise | Eliminate arcing from brushes to commutator. |
| Reduced acoustic noise | Eliminate brush bounce, especially at high speeds. |
| Reduced debris | Eliminate brush wear. |
| Increased speed range | Remove mechanical limitations imposed by brush / commutator interface. |
| Reduced size due to superior thermal characteristics | Brushless motors have windings on the stator; brush motors have windings on rotor. Windings are the main heat generators on PM motors and it is easier to remove heat from the stator than from the rotor, if stator is the outer part of the machine |
| Reduced maintenance | Eliminate brush wear. |
| Reduced weight and size | Eliminate commutator, brush, and brush holders. |
| Improved MTBF | Reduce parts count and electrical interconnects by eliminating mechanical commutation. |

Some advantages directly impact overall machine cost. For example, lighter motors require less structural support. Higher efficiency motors require a smaller power stage or may eliminate the need for cooling fans. Relocating the motor without concern for brush debris may reduce the cost of mechanical structures.

Other advantages are important because they add value to the machine. For example eliminating brush noise may take the machine run more quietly. Eliminating brushes increases reliability and can reduce the machine's scheduled maintenance cost. Other features such as improved efficiency, elimination of brush debris or reduced electrical noise may all be important beyond direct cost impact (Ellis, G., 1996).

The contents of this thesis can be summarized briefly as follows:

In second chapter, the brushless DC motor is introduced. Construction of the BLDC motors is explained. Six-pulse inverter model and its equations are defined. Then torque profiles in BLDC motors are presented. After that torque/speed characteristic is given.

Chapter 3 provides the mathematical model of brushless DC motor. That means the circuit equations of the three windings in phase variables; electromagnetic torque and rotor position are defined. Next, the motor parameters are measured.

The fourth chapter is devoted to brushless DC drive circuit TDA5142T (Philips). The operation principle is explained; the components, which should be determined, are defined.

In Chapter 5, simulation results and experimental results are given. Computer simulation prepared in Matlab for P-pole pair machine. The implemented circuit is designed by using TDA5142T. The simulation results are compared to experimental results. Moreover, closed loop control is applied to the brushless DC motor.

Chapter 6 is concerned with the conclusions.

# CHAPTER TWO

# BRUSHLESS DC MOTOR

The construction of modern brushless motors is very similar to the ac motor, known as the permanent magnet synchronous motor. Figure 2.1 illustrates the structure of a typical three-phase brushless DC motor. The stator windings are similar to those in a polyphase ac motor, and the rotor is composed of one or more permanent magnets. Brushless DC motors require some form of rotor position transformer in order to select the correct commutation sequence as shown in Figure 2.2. The most common position sensor is the Hall element, but some motors use optical sensors (Kenyo, T., & Nagamori, S., 1985). However, in practice, the rotor position sensors have limited resolution and operating characteristics, and they are sensitive to environmental conditions. The position sensor also constitutes a substantial fraction of the total drive cost and tends to reduce the drive reliability. Moreover, the available space might make difficult the use of mechanical shaft position sensors in some of the drive systems. Because of these drawbacks, shaft position sensor elimination techniques have received attention within the last decade. Direct back emf detection is most popular method of the sensorless control (Ertugrul, N., & Acarnley, P.P., 1998).
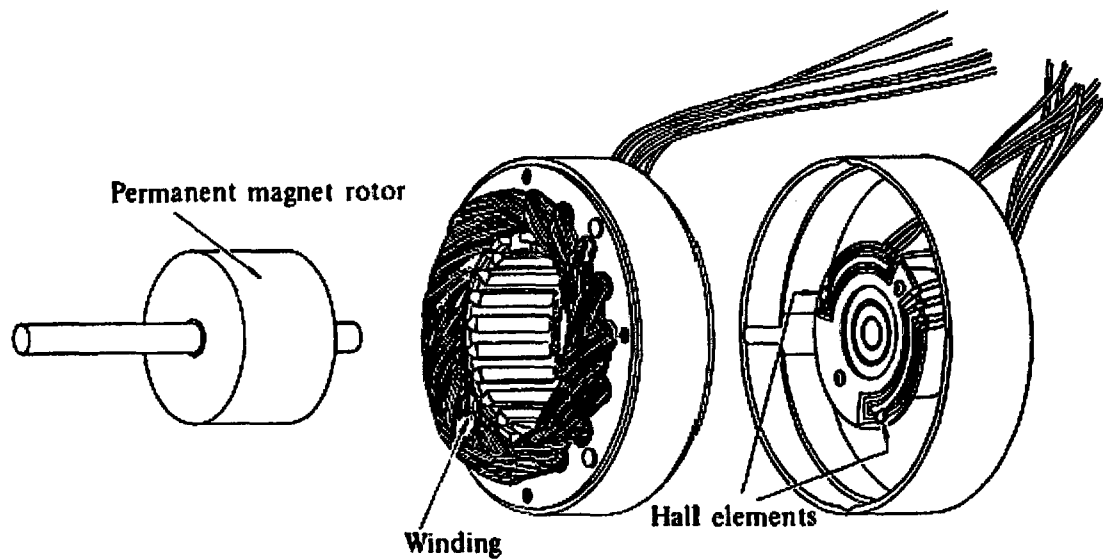
**Figure 2.1 Disassembled view of a brushless DC (BLDC) motor**
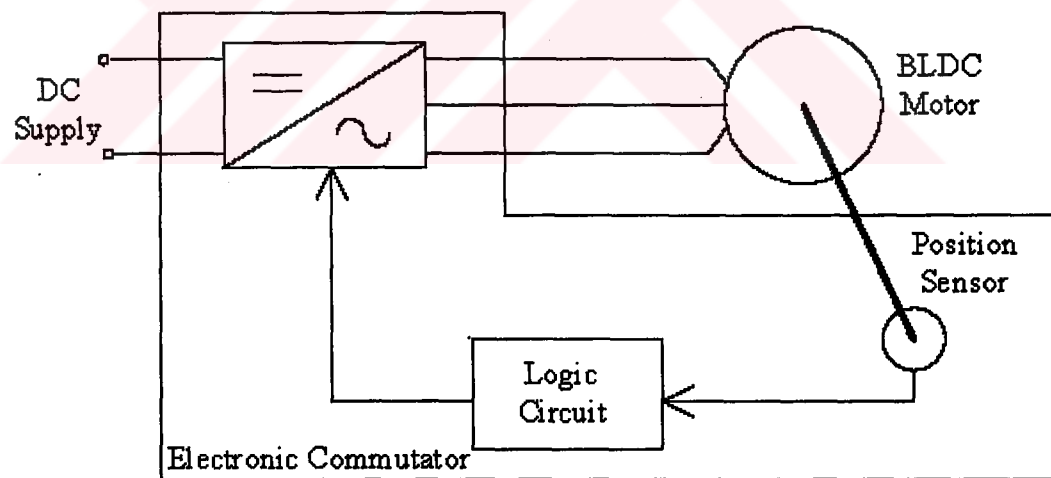


**Figure 2.2 BLDC motor and electronic commutator**

## 2.1 Controllers for Brushless DC Motors

Controllers for permanent magnet BLDC motors are more complex than the conventional dc motors. The reason of that is providing both torque control and electronic commutation. A three-phase full bridge inverter shown in the Figure 2.3 is used in the control circuit. Inverters are known as dc-to-ac converters. The function of an inverter is to change a dc input voltage to a symmetrical ac output voltage of desired magnitude and frequency. The output voltage could be fixed or variable at a fixed or variable frequency (Rashid, M.H., 1993).

The inverter may be operated the $120^{\circ}$ or $180^{\circ}$ conduction modes depending on the machine design and the desired current waveshape. This study will focus on the $120^{\circ}$ conduction mode.

## 2.1.1 Six-Pulse Inverter Model ($120^{\circ}$ conduction mode)

It is also called six-step discontinuous current inverter. The following voltage equations may be written by using Figure 2.3.

$$V_{ap} = V_{an} + V_{np} \tag{2.1}$$

$$V_{bp} = V_{bn} + V_{np} \tag{2.2}$$

$$V_{cp} = V_{cn} + V_{np} \tag{2.3}$$
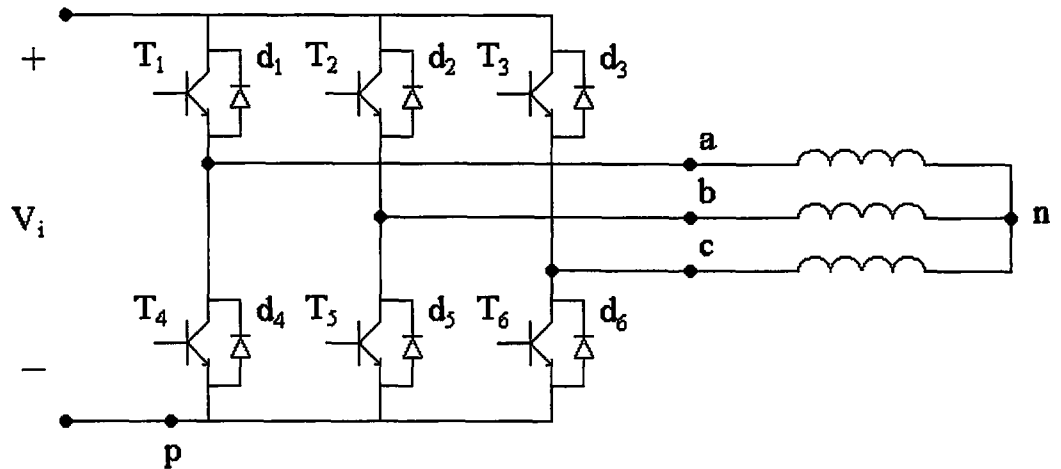
**Figure 2.3 Schematic of three phase inverter**

The stator is connected as a three-wire system whereupon the sum of $V_{an}$, $V_{bn}$, and $V_{cn}$ is zero. Thus

$$V_{np} = (V_{ap} + V_{bp} + V_{cp}) / 3. \tag{2.4}$$

Hence

$$V_{an} = 2V_{ap} / 3 - (V_{bp} + V_{cp}) / 3 \tag{2.5}$$

$$V_{bn} = 2V_{bp} / 3 - (V_{ap} + V_{cp}) / 3 \tag{2.6}$$

$$V_{cn} = 2V_{cp} / 3 - (V_{ap} + V_{bp}) / 3 \tag{2.7}$$

where $V_{ap}$, $V_{bp}$, and $V_{cp}$ are either $V_i$ or zeros depending upon the state of $T_1$ - $T_6$.

In this type of inverter, each transistor conducts for $120°$. Only two transistors remain on at any instant of time. If the power factor at the output of the inverter is high, then the phase currents become discontinuous. During periods, in which a phase current is zero, the phase back emf voltage appears at terminals of the BLDC motor. In Table 2.1 is shown the switching sequence of the transistors.

**Table 2.1 Conduction sequences of the transistors**

| Conduction Sequences | Transistors | | | | | |
|:---:|:---:|:---:|:---:|:---:|:---:|:---:|
| | $T_1$ | $T_2$ | $T_3$ | $T_4$ | $T_5$ | $T_6$ |
| 1 | ON | OFF | OFF | OFF | OFF | ON |
| 2 | OFF | ON | OFF | OFF | OFF | ON |
| 3 | OFF | ON | OFF | ON | OFF | OFF |
| 4 | OFF | OFF | ON | ON | OFF | OFF |
| 5 | OFF | OFF | ON | OFF | ON | OFF |
| 6 | ON | OFF | OFF | OFF | ON | OFF |

It is constructive to consider the action of one leg of the inverter. For Example, $T_1$ and $T_4$. Transistor $T_1$ conducts for $120°$. When transistor $T_1$ is turned off, T4 is not turned on until $60°$ later. It is natural time delay.

**Conduction Sequence 1:**

$V_{ap} = V_i$

$V_{cp} = 0$

if $i_b$ is less than zero, then $V_{bp} = V_i$ ($d_2$ is conducting)

$i_i = i_a$

**Conduction Sequence 2:**

$V_{bp} = V_i$

$V_{cp} = 0$

if $i_a$ is greater than zero, then $V_{ap} = 0$ ($d_4$ is conducting)

$i_i = i_b$

### Conduction Sequence 3:

$V_{ap} = 0$

$V_{bp} = V_i$

if $i_c$ is less than zero, then $V_{cp} = V_i$ ($d_3$ is conducting)

$i_i = i_b$

### Conduction Sequence 4:

$V_{ap} = 0$

$V_{cp} = V_i$

if $i_b$ is greater than zero, then $V_{bp} = 0$ ($d_5$ is conducting)

$i_i = i_c$

### Conduction Sequence 5:

$V_{bp} = 0$

$V_{cp} = V_i$

if $i_a$ is less than zero, then $V_{ap} = V_i$ ($d_1$ is conducting)

$i_i = i_c$

### Conduction Sequence 6:

$V_{ap} = V_i$

$V_{bp} = 0$

if $i_c$ is greater than zero, then $V_{cp} = 0$ ($d_6$ is conducting)

$i_i = i_a$

In application of the discontinuous current inverter, each phase floats twice during each main cycle. Therefore one phase of the BLDC motor is open during this time.

For example, when "phase a" is open-circuited, $i_a$ is equal to zero, then $V_{an}$ is equal to back emf voltage of this phase (The Electric Power Research Institute and The Entergy Corporation).

## 2.2 Torque Profiles in PM Brushless DC Motors

In rotating machines two MMFs displaced by a fixed nonzero angle rotate in the air-gap for torque production. If this angle and the MMF magnitudes are constant, then the torque produced will also be constant.

$$T_{em} = K \, M_R \, M_S \, \sin \theta \tag{2.8}$$

where

$T_{em}$ is the electromagnetic torque,

K is a constant,

$M_R$ is the magnitude of the MMF produced by the rotor,

$M_S$ is the magnitude of the MMF produced by the stator, and

$\theta$ is the angle between the two MMFs.

In PM BLDC motors these MMFs must rotate at synchronous speed due to the moving magnets in order to produce a non-zero average torque. This is accomplished by synchronizing the inverter switching to the position of the rotor. From 120° conduction inverters, this result in a balanced three phase set currents as shown in idealized form in Figure 2.4
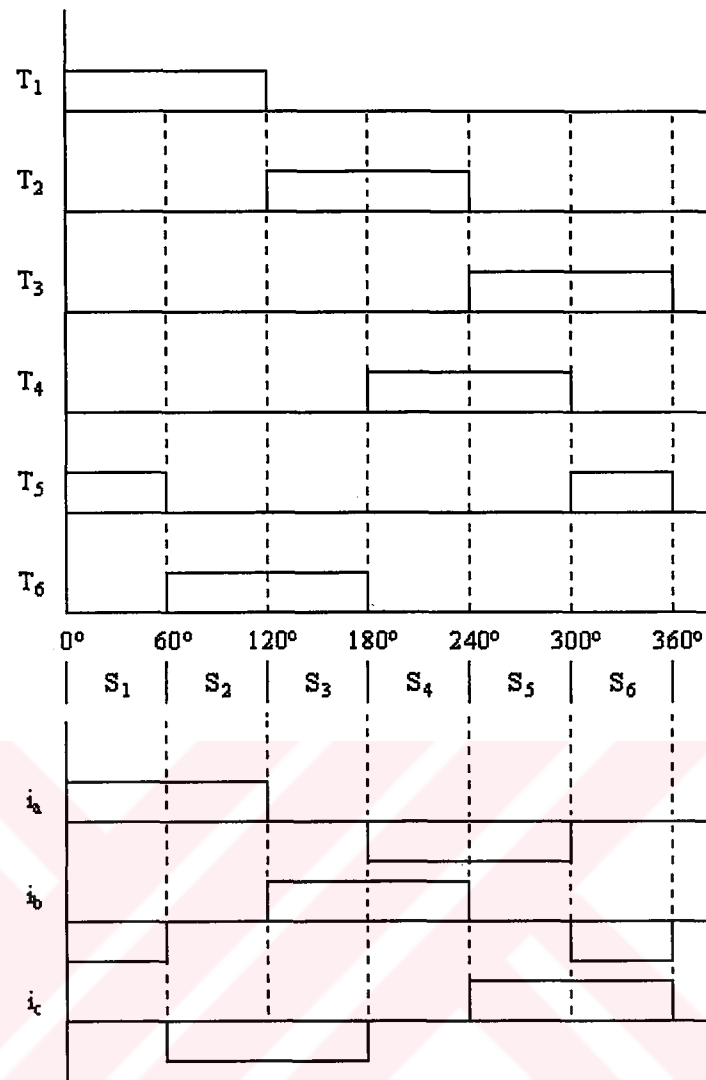
**Figure 2.4 Phase currents, 120° conduction mode**

The MMF produced by these currents is stationary during the entry duration of a state. It is only at the transition between two states that the MMF moves the sixty electrical degrees into the next state.

The nature of these pulsations can be determined using the torque expressions given in Equation (2.8). To maximize the torque/ampere of the machine, the average torque angle should be equal to 90 electrical degrees. This is achieved by beginning each state with an angle of 120° between the MMFs and ending with 60°. The torque at the beginning of each state is therefore

$$T_{em} = K \, M_R \, M_S \, \sin(120°) = \frac{\sqrt{3}}{2} \, K \, M_R \, M_S. \tag{2.9}$$

At the middle of each state the torque increases to

$$T_{em} = K \, M_R \, M_S \, \sin(90°) = K \, M_R \, M_S. \tag{2.10}$$

At end of the state the torque drops back to its initial value

$$T_{em} = K \, M_R \, M_S \, \sin(60°) = \frac{\sqrt{3}}{2} \, K \, M_R \, M_S. \tag{2.11}$$

These relationships are displayed in Figure 2.5.
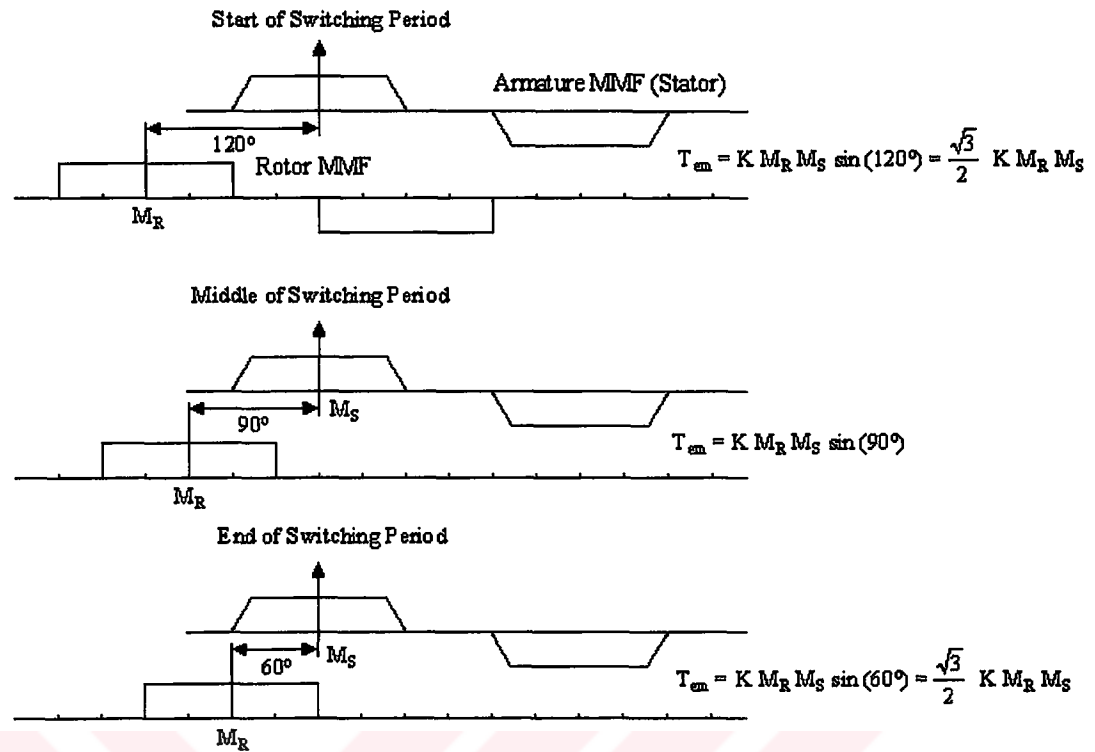
**Figure 2.5 MMF, torque at start, middle, end of switching period**

The expected torque profile is given in Figure 2.6 (Nehl, T.W., & Demerdash, N.A., 1992).
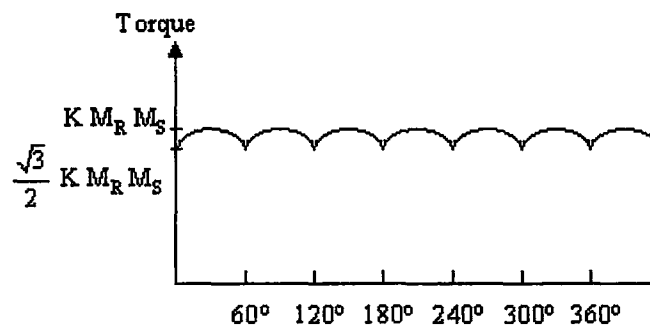


**Figure 2.6 Idealized BLDC motor torque profile**

There are many literatures, using new control techniques, to minimize torque ripples. A number of schemes have been suggested. Berendsen, Champenois, and Bolopion reduce the ripples by compensation the $V_{NO}$ voltage, where O is the midpoint of the dc supply and N is the neutral point of the machine (Brendsen, et al., 1993).

S.J. Park, H.W. Park, Lee, and Harashima applied a novel approach to achieve ripple-free torque control with maximum efficiency based on the *d-q-0* reference frame is presented. The proposed method optimizes the reference phase current waveforms, which include the case of three-phase unbalanced conditions. The proposed approach provides a simple way to obtain optimal motor excitation currents (S.J. Park, et al, 2000).

## 2.3 Torque/Speed Characteristic

The flux linkage with the phase winding varies linearly with the rotor position $\theta$ and is given by

$$\lambda(\theta) = \left(1 - \frac{2}{\pi}\theta\right)\lambda_m \qquad (2.12)$$

where $\lambda_m$ is the maximum flux linkage. It is equal to

$$\lambda_m = N_1\, B_{mag}\, \tau\, l_s \qquad (2.13)$$

where

$N_1$ = number of turns/phase,

$B_{mag}$ = airgap flux density produced by the PM,

$\tau$ = pole pitch,

$l_s$ = stator stack length.

The voltage induced in a phase due to the flux linkage becomes:

$$E_a = -\frac{d\lambda}{dt} = -\frac{d\lambda}{d\theta}\frac{d\theta}{dt} = \frac{2}{\pi}\lambda_m \omega_r \qquad (2.14)$$

where $\omega_r$ is rotor angular speed in electrical radians per second. The developed electromagnetic torque, $T_e$ is given by

$$T_e = 2\ E_a\ I_{dc}\ \frac{P}{\omega_r} = \frac{4}{\pi}\ P\ \lambda_m\ I_{dc} \qquad (2.15)$$

where P is number of pole pairs.

The commutation of current is instantaneous, and the stator inductance voltage drop may be neglected. Thus, under steady state the voltage equation for the motor may be expressed as

$$V = 2\ R_s\ I_{dc} + 2\ E_a = 2\ R_s\ I_{dc} + \frac{4}{\pi}\ \lambda_m\ \omega_r \qquad (2.16)$$

where $R_s$ is phase resistance, and V is the terminal voltage.

Using the equations (2.15) and (2.16) together, the torque/speed characteristic can be derived as:

$$\omega_r = \omega_0 \left(1 - \frac{T_e}{T_{esc}}\right) \qquad (2.17)$$

where $\omega_0$ is no-load speed and equal to

$$\omega_o = \frac{\pi V_o}{4\lambda_m}$$
(2.18)

$T_{esc}$ is the torque with motor stalled, i.e. at zero speed, and it is given by

$$T_{esc} = \frac{4}{\pi} P \lambda_m I_{sc}$$
(2.19)

$I_{sc}$ is the stall current.

$$I_{sc} = \frac{V}{2R}$$
(2.20)

This characteristic is similar to that of a shunt dc motor. The machine back emf is a linear function of the machine speed, which is essentially controlled by the voltage V. The voltage is usually controlled by chopping or PWM (Miller, T.J.E., 1989).

# CHAPTER THREE

# BRUSHLESS DC MOTOR MODELLING

## 3.1 Mathematical Model of the Brushless DC Motor

The brushless DC (BLDC) motor has three stator windings and permanent magnets on the rotor. Since both the magnet and the stainless-steel retaining sleeves have high resistivity, rotor-induced currents can be neglected and no damper windings are modeled. Hence the circuit equations of the three windings in phase in phase variables are (Pillay, P., & Krishnan R., 1989).

$$
\begin{bmatrix} V_{AS} \\ V_{BS} \\ V_{CS} \end{bmatrix} = \begin{bmatrix} R_a & 0 & 0 \\ 0 & R_b & 0 \\ 0 & 0 & R_c \end{bmatrix} \begin{bmatrix} i_a \\ i_b \\ i_c \end{bmatrix} + \frac{d}{dt} \begin{bmatrix} L_a & L_{ab} & L_{ac} \\ L_{ba} & L_b & L_{bc} \\ L_{ca} & L_{cb} & L_c \end{bmatrix} \begin{bmatrix} i_a \\ i_b \\ i_c \end{bmatrix} + \begin{bmatrix} e_a \\ e_b \\ e_c \end{bmatrix}
$$

(3.1)

where

$R_a$, $R_b$, $R_c$: Resistances of each phase ($\Omega$),

$L_a$, $L_b$, $L_c$: Self-inductances of each phase (H),

$L_{ab}$, $L_{bc}$, $L_{ca}$: Mutual inductances of between phases (H),

$e_a$, $e_b$, $e_c$: The electromotive forces (emf) for phases a, b, c (V),

$V_{AS}$, $V_{BS}$, $V_{CS}$: Stator phase voltages (V),

$i_a$, $i_b$, $i_c$: Currents through the phases a, b, c (A).

Equivalent circuit diagram of the three-phase star connected BLDC motor is shown in Figure 3.1.
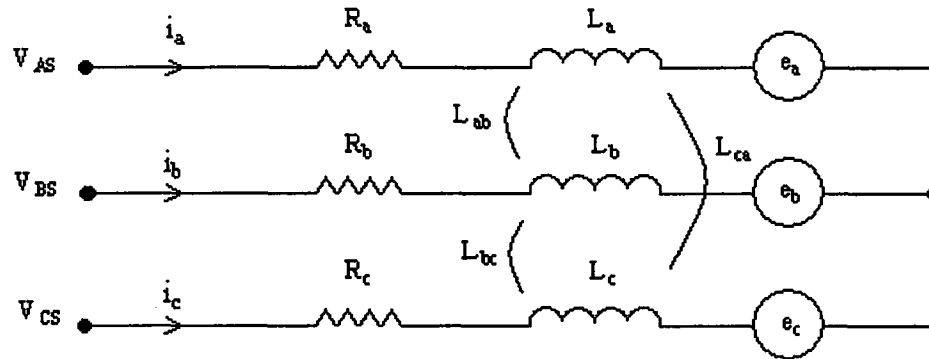
**Figure 3.1 Equivalent circuit of BLDC motor**

It has been assumed that the stator resistances of all the windings are equal. Back emfs, $e_a$, $e_b$, $e_c$, have trapezoidal shapes as shown in Figure 3.2.

Assuming further that there is no change in the rotor reluctances, then

$L_a = L_b = L_c = L$,

$L_{ab} = L_{bc} = L_{ca} = M$. 								(3.2)

Hence

$$\begin{bmatrix} V_{AS} \\ V_{BS} \\ V_{CS} \end{bmatrix} = \begin{bmatrix} R & 0 & 0 \\ 0 & R & 0 \\ 0 & 0 & R \end{bmatrix} \begin{bmatrix} i_a \\ i_b \\ i_c \end{bmatrix} + \frac{d}{dt} \begin{bmatrix} L & M & M \\ M & L & M \\ M & M & L \end{bmatrix} \begin{bmatrix} i_a \\ i_b \\ i_c \end{bmatrix} + \begin{bmatrix} e_a \\ e_b \\ e_c \end{bmatrix}$$								(3.3)

but the sum of $i_a$, $i_b$, $i_c$ are zero, therefore,

$M\,i_b + M\,i_c = -Mi_a$. 								(3.4)

Hence

$$
\begin{bmatrix} V_{AS} \\ V_{BS} \\ V_{CS} \end{bmatrix} = \begin{bmatrix} R & 0 & 0 \\ 0 & R & 0 \\ 0 & 0 & R \end{bmatrix} \begin{bmatrix} i_a \\ i_b \\ i_c \end{bmatrix} + \frac{d}{dt} \begin{bmatrix} L-M & 0 & 0 \\ 0 & L-M & 0 \\ 0 & 0 & L-m \end{bmatrix} \begin{bmatrix} i_a \\ i_b \\ i_c \end{bmatrix} + \begin{bmatrix} e_a \\ e_b \\ e_c \end{bmatrix}
$$

(3.5)

and the electromagnetic torque is

$$
T_e = \frac{(e_a i_a + e_b i_b + e_c i_c)}{\omega_m}
$$

(3.6)

or

$$
T_e = J \frac{d\omega_m}{dt} + B\omega_m + T_L
$$

(3.7)

where

$T_e$: electromagnetic torque (Nm),

$\omega_m$: rotor angular speed in mechanical radians per second,

J: moment of inertia (kg.m$^2$),

B: damping ratio,

P: number of pole pairs,

$T_L$: Load torque (Nm).

Rotor position:

$$
\theta_m = \int_0^t \omega_m dt
$$

(3.8)

To control the torque, it is necessary that the stator currents strictly follow the square references shown in Figure 3.2. The amplitudes of the currents are proportional to the desired torque, and their phases are tied to the rotor position (Brendsen, et al., 1993).
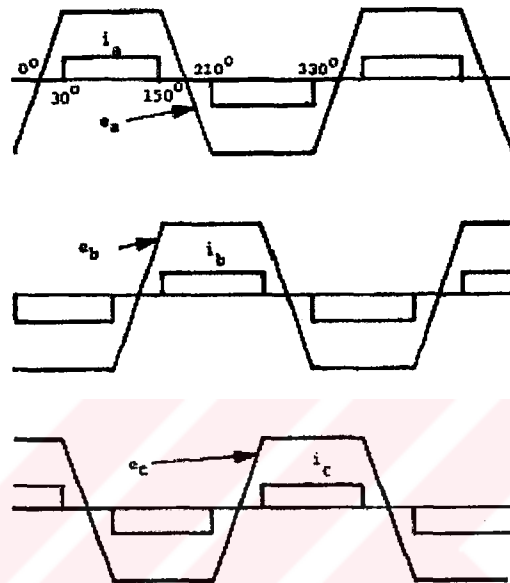


**Figure 3.2 Ideal shapes of the emfs and the currents**

## 3.2 Measurement of the Motor Parameters

Before using the mathematical model of BLDC motor in a computer program, it is necessary to know motor parameters. In this study, the basic motor parameters are practically measured, using the techniques described in (Wu, M., 1992).

### 3.2.1 Stator Winding Resistance Measurement

The circuit is set up as shown in Figure 3.3, V is an adjustable dc source and A is an ammeter.
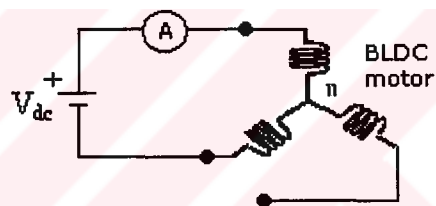


**Figure 3.3 Circuit for measuring resistance**

The result is $V_{dc}$ =0.2 V, I = 0.6 A,

Hence

$$R = \frac{V_{dc}}{2 \times I} = \frac{0.2}{2 \times 0.6} = 0.167 \ \Omega \tag{3.9}$$

### 3.2.2 Stator Winding Inductance Measurement

The circuit in Figure 3.4 is used to measure the stator winding inductance. The switch S is turned off and on for a moment. It could be seen an exponential response curve at the current. This curve is used to calculate the time constant and the inductance value can be determined from the time constant and winding resistance.
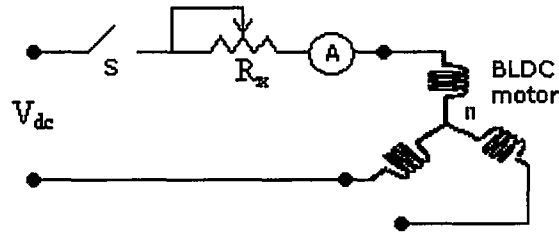


**Figure 3.4 Circuit for measuring inductance**

From Figure 3.5, the current reaches its steady state value in $5\tau$ seconds. $\tau$ is the time constant, which is equal to $\dfrac{2(L-M)}{R_x + 2R}$. Hence

$$5\tau = 0.3m\sec \Rightarrow \tau = 60\mu\sec \tag{3.10}$$

$$\text{also } \tau = \frac{2(L-M)}{R_x + 2R} \tag{3.11}$$

where $R_x = 7\ \Omega$ and R=0.167 $\Omega$, from equation 3.11,

therefore L-M = 210 µH.
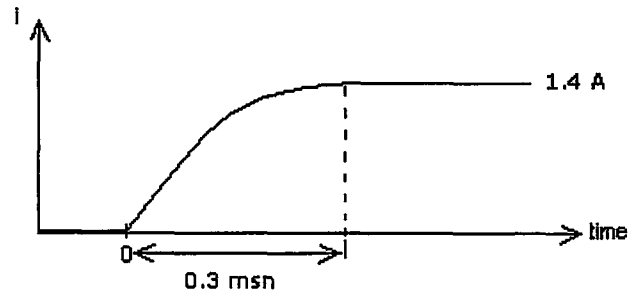
**Figure 3.5 Current vs. time**

### 3.2.3 Back Emf and Torque Constant Measurement

The rotor of BLDC motor is connected to the rotor of another motor, and this drives BLDC motor. Because of the permanent magnet rotor, the back emf is induced in the stator windings while running. The back emf is computed from the following equations:

$$e_a = K_T \omega_m \tag{3.12}$$

**Table 3.1 Back emf and torque constant**

| Mechanical Speed, $\omega_m$ (rad/sec) | Back emf, $e_a$ (V) | Torque Constant, $K_T$ (V/rad/sec) |
|---|---|---|
| 19.64 | 0.5 | 0.025 |
| 20.94 | 0.6 | 0.03 |

# CHAPTER FOUR

# BRUSHLESS DC MOTOR DRIVE CIRCUIT

# TDA5142T

## 4.1 Introduction

Full-wave driving of a three-phase motor requires three push-pull output stages. In each of the six possible states two outputs are active, one sourcing (H) and one sinking (L). The third output presents a high-impedance (Z) to the motor, which enables measurement of the motor back-emf in the corresponding motor coil by the emf comparator at each output. The commutation logic is responsible for control of the output transistors and selection of the correct emf comparator. In Table 4.1 the sequence of the six possible states of the external connected output transistors has been depicted and the corresponding output levels on the NA, PA, NB, PB, NC and PC outputs of the TDA5142T, shown in the Figure 4.1.

The zero crossing in the motor emf (detected by the comparator selected by the commutation logic) is used to calculate the correct moment for the next commutation, that is, the change to the next output state. The delay is calculated (depending on the motor loading) by the adaptive commutation delay block. The output stages are also protected by a current limiting circuit and by thermal protection.

The detected zero-crossings are used to provide speed information. The information has been made available on the FG output pin. This output provides an output signal with a frequency equal to the commutation frequency.
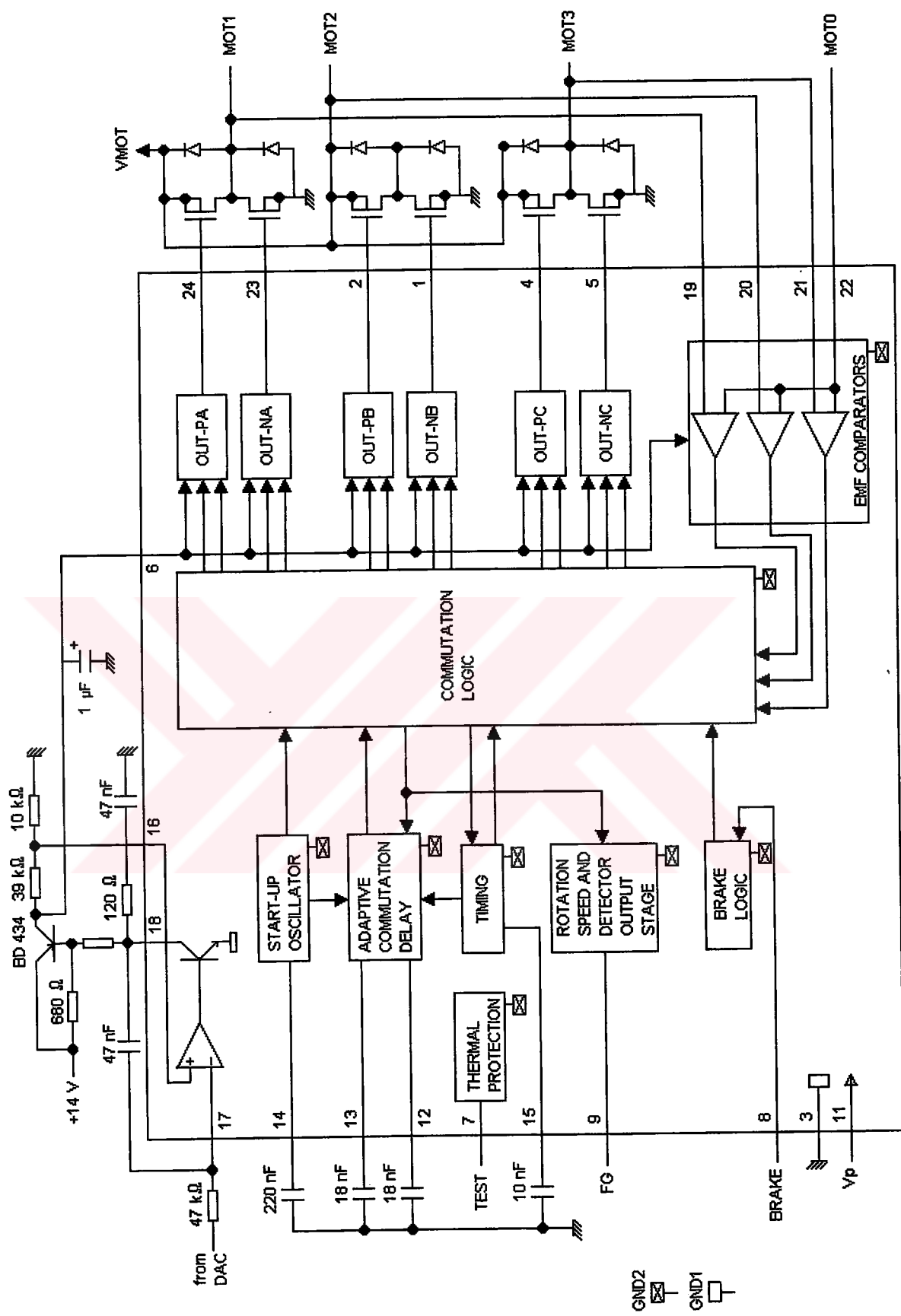
**Figure 4.1 Typical application of the TDA5142T as a scanner driver, with use of OTA**

The system will only function when the emf voltage from the motor is present. Therefore, a start oscillator is provided that will generate commutation pulses when no zero-crossings in the motor voltage are available.

A timing function is incorporated into the device for internal timing and for timing of the reverse rotation detection. The TDA5142T also contains an uncommitted transconductance amplifier (OTA) that can be used as a control amplifier. The output is capable of directly driving an external power transistor. The TDA5142T is designed for systems with low current consumption: use of "$I^2L$" logic, adaptive base drive for the output transistors (patented).

**Table 4.1 Output States**

| STATE | MOT1 | OUT-NA | OUT-PA | MOT2 | OUT-NA | OUT-PA | MOT3 | OUT-NA | OUT-PA |
|-------|------|------|------|------|------|------|------|------|------|
| 1 | Z | L | H | L | H | H | H | L | L |
| 2 | H | L | L | L | H | H | Z | L | H |
| 3 | H | L | L | Z | L | H | L | H | H |
| 4 | Z | L | H | H | L | L | L | H | H |
| 5 | L | H | H | H | L | L | Z | L | H |
| 6 | L | H | H | Z | L | H | H | L | L |

**Note:** H= HIGH state; L= LOW state; Z= high impedance OFF-state

## 4.2 Adjustments

The system has been designed in such a way that the tolerances of the application components are not critical. However, the approximate values of the following components must still be determined:

- The start capacitor; this determines the frequency of the start oscillator.
- The two capacitors in the adaptive commutation delay circuit; these are important in determining the optimum moment for commutation, depending on the type and loading of the motor.
- The timing capacitor; this provides the system with its timing signals.

### 4.2.1 The Start Capacitor (CAP-ST)

This capacitor determines the frequency of the start oscillator. It is charged and discharged, with a current of 2 µA, from 0.05 to 2.2 V and back to 0.05 V. The time taken to complete one cycle is given by:

$$t_{start} = (2.15 \times C) \sec \quad \text{(with C in µF)} \tag{4.1}$$

The start oscillator is reset by a commutation pulse and so is only active when the system is in the start-up mode. A pulse from the start oscillator will cause the outputs to change to the next state (torque in the motor).

If the movement of the motor generates enough emf the TDA5142T will run the motor. If the amount of emf generated is insufficient, then the motor will move one step only and will oscillate in its new position. The amplitude of the oscillation must decrease sufficiently before the arrival of the next start pulse, to prevent the pulse arriving during the wrong phase of the oscillation. The oscillation of the motor is given by:

$$f_{osc} = \frac{1}{2\pi\sqrt{\dfrac{K_t \times I \times p}{J}}}$$

(4.2)

where:

$K_t$ = Torque constant (Nm/A)

$I$ = Current (A)

$p$ = Number of magnetic pole-pairs

$J$ = Inertia $J$ (kg.m$^2$).

Example: J = 72 × 10$^{-6}$ kg.m$^2$, K$_t$ = 25 × 10$^{-3}$ Nm/A, p = 6 and I = 0.5 A; this gives f$_{osc}$ = 5 Hz. If the damping is high then a start frequency of 2 Hz can be chosen or t = 500 ms, thus C = 0.5/2 = 0.25 μF (choose 220 nF).

### 4.2.2 The Adaptive Commutation Delay (CAP-CD and CAP-DC)

In this circuit capacitor CAP-CD is charged during one commutation period, with an interruption of the charging current during the diode pulse. During the next commutation period this capacitor (CAP-CD) is discharged at twice the charging current. The charging current is 8.1 μA and the discharging current 16.2 μA; the voltage range is from 0.9 to 2.2 V. The voltage must stay within this range at the lowest commutation frequency of interest, f$_{C1}$:

$$C = \frac{8.1 \times 10^{-6}}{f \times 1.3} = \frac{6231}{f_{C1}} \quad \text{(C in nF)}$$

(4.3)

If the frequency is lower, then a constant commutation delay after the zero-crossing is generated by the discharge from 2.2 to 0.9 V at 20 μA;

maximum delay $= ( 0.076 \times C )$ ms (with $C$ in nF) (4.4)

Example: Nominal commutation frequency is 900 Hz and the lowest usable frequency is 400 Hz; so:

$$\text{CAP-CD} = \frac{6231}{400} = 15.6 \text{ nF} \quad (\text{choose } 18 \text{ nF}) \tag{4.5}$$

The other capacitor, CAP-DC, is used to repeat the same delay by charging and discharging with 15.5 µA. The same value can be chosen as for CAP-CD. Figure 4.2 illustrates typical voltage waveforms.
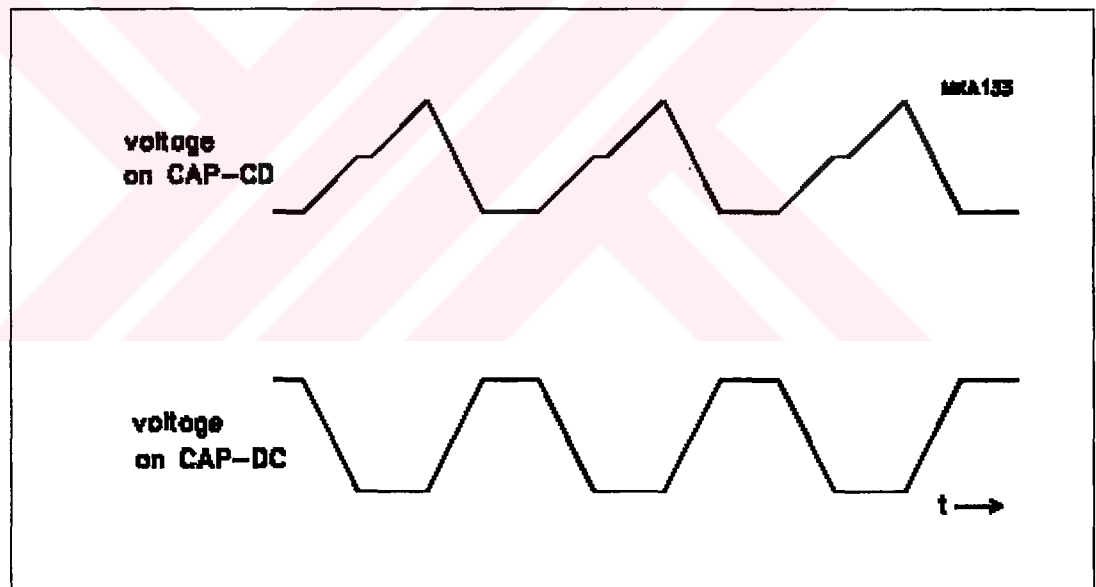


**Figure 4.2 CAP-CD and CAP-DC typical voltage waveform in normal running mode.**

### 4.2.3 The Timing Capacitor (CAP-TI)

Capacitor CAP-TI is used for timing the successive steps within one commutation period; these steps include some internal delays. The most important function is the watchdog time in which the motor emf has to recover from a negative diode-pulse back to a positive emf voltage (or vice versa). A watchdog timer is a guarding function that only becomes active when the expected event does not occur within a predetermined time.

The emf usually recovers within a short time if the motor is running normally (<<ms). However, if the motor is motionless or rotating in the reverse direction, then the time can be longer (>>ms). A watchdog time must be chosen so that it is long enough for a motor without emf (still) and eddy currents that may stretch the voltage in a motor winding; however, it must be short enough to detect reverse rotation. If the watchdog time is made too long, then the motor may run in the wrong direction (with little torque).

The capacitor is charged, with a current of 57 µA, from 0.2 to 0.3 V. Above this level it is charged, with a current of 5 µA, up to 2.2 V only if the selected motor emf remains in the wrong polarity (watchdog function). At the end, or, if the motor voltage becomes positive, the capacitor is discharged with a current of 28 µA. The watchdog time is the time taken to charge the capacitor, with a current of 5 µA, from 0.3 to 2.2 V.

To ensure that the internal delays are covered CAP-TI must have a minimum value of 2 nF. For the watchdog function a value for CAP-TI of 10 nF is recommended. To ensure a good start-up and commutation, care must be taken that no oscillations occur at the trailing edge of the flyback pulse. Snubber networks at the outputs should be critically damped. Figure 4.3 illustrates typical voltage waveforms.
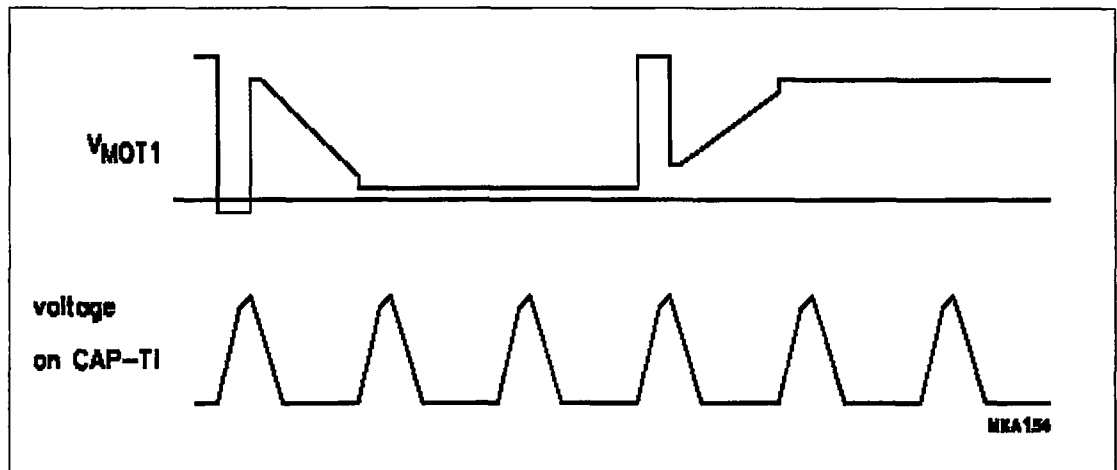
**Figure 4.3 Typical CAP-TI and $V_{MOT1}$ voltage waveforms in normal running mode**

If the chosen value of CAP-TI is too small oscillations can occur in certain positions of a blocked rotor. If the chosen value is too large, then it is possible that the motor may run in the reverse direction (synchronously with little torque).

## 4.3 Other Design Aspects

There are other design aspects concerning the application of the TDA5142T besides the commutation function. They are:

- Generation of the tacho signal FG
- General purpose operational transconductance amplifier (OTA)
- Possibilities of motor control
- Brake function
- Reliability.

### 4.3.1 FG Signal

The FG signal is generated in the TDA5142T by using the zero crossing of the motor emf from the three motor windings and the commutation signal. Output FG switches from HIGH-to-LOW on all zero crossings and from LOW-to-HIGH on all commutations. Output FG can source typically 75 $\mu$A and sink more than 3 mA.

Example: A 3-phase motor with 6 magnetic pole-pairs at 1500 rpm and with a full-wave drive has a commutation frequency of $25 \times 6 \times 6 = 900$ Hz, and generates a tacho signal of 900 Hz.

### 4.3.2 The Operational Transconductance Amplifier (OTA)

The OTA is an uncommitted amplifier with a high output current (40 mA) that can be used as a control amplifier. The common mode input range includes ground (GND) and rises to $V_P$-1.7 V. The high sink current enables the OTA to drive a power transistor directly in an analog control amplifier.

Although the gain is not extremely high (0.3 S), care must be taken with the stability of the circuit if the OTA is used as a linear amplifier as no frequency compensation has been provided. The convention for the inputs (inverting or not) is the same as for a normal operational amplifier: with a resistor (as load) connected from the output (AMP OUT) to the positive supply, a positive-going voltage is found when the non-inverting input (+AMP IN) is positive with respect to the inverting input (-AMP IN). Confusion is possible because a 'plus' input causes less current, and so a positive voltage.

### 4.3.3 Motor Control

DC motors can be controlled in an analog manner using the OTA. For the analog control an external transistor is required. The OTA can supply the base current for this transistor and act as a control amplifier shown in Figure 4.1.

### 4.3.4 Brake Function

If the voltage on pin 8 is < 2.3 V the motor brakes; in this condition the external outputs are driven to a HIGH voltage level. If pin 8 is floating or the voltage is > 2.7 V the motor runs normally.

### 4.3.5 Reliability

It is necessary to protect high current circuits and the output stages are protected in two ways:

- Current limiting of the 'lower' output transistors. The 'upper' output transistors use the same base current as the conducting 'lower' transistor (+15%). This means that the current to and from the output stages is limited.
- Thermal protection of the six output transistors is achieved in such a way that the transistors are switched off when the local temperature becomes too high (TDA5142T Brushless DC Motor Drive Circuit, 1994)

# CHAPTER FIVE

# SIMULATION RESULTS AND EXPERIMENTAL RESULTS

### 5.1 Simulation Results of Brushless DC Motor

Modern motors and also power components are designed and analyzed by using computer simulation as a tool for conducting transients and control studies. Simulation can be especially helpful about the dynamic behavior and interactions that are often not readily apparent from reading theory. Simulation is often chosen by engineers to study transient and control performance or to test conceptual designs, before the experiment of actual system (Ong, C., 1998).

According to the mathematical model of the BLDC motor, which is explained in Chapter Three, the computer simulation program is prepared in Matlab for the P-pole pair machine. The block diagram of the BLDC using in computer simulation is shown in Figure 5.1.
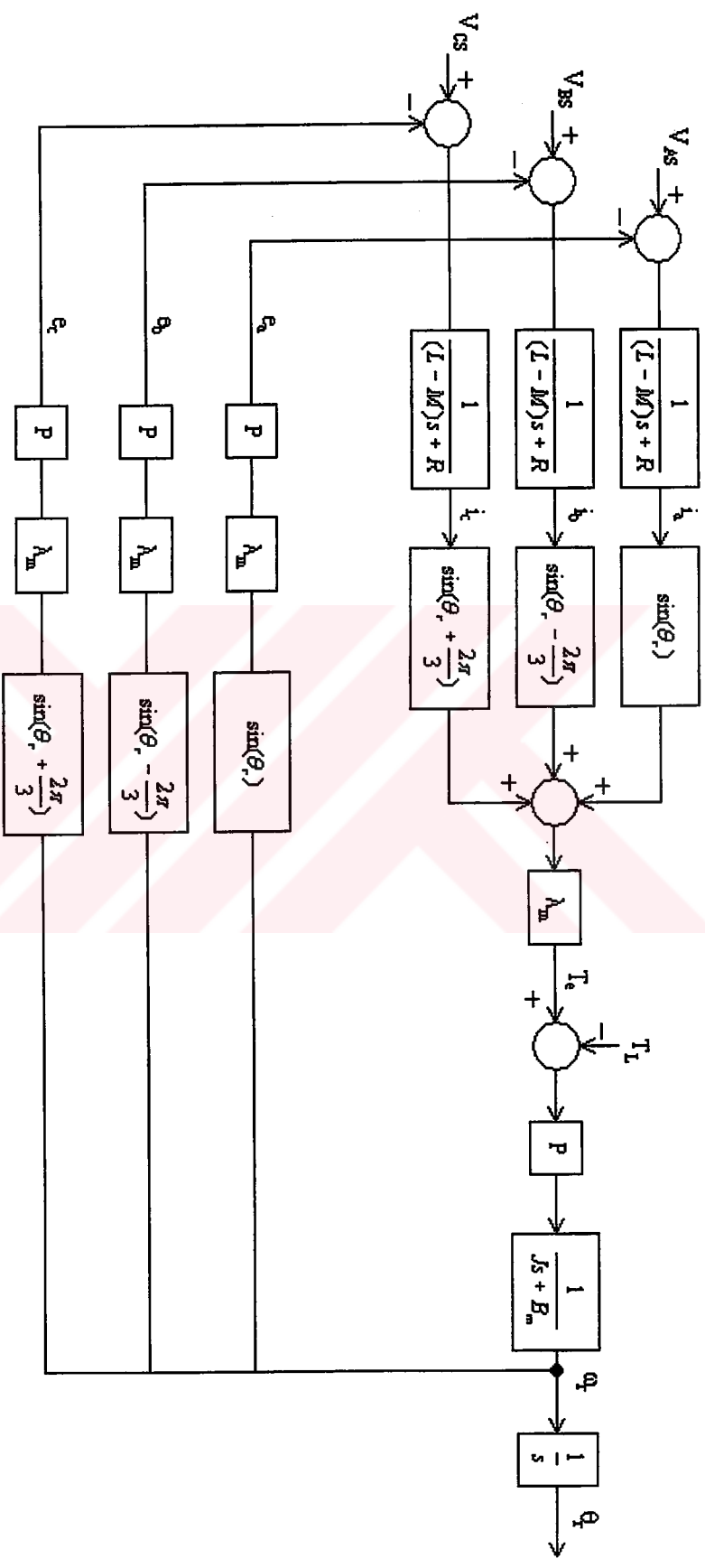
**Figure 5.1 Block diagram of the P-pole pair BLDC motor**

In Figure 5.1 $\omega_r$ is rotor angular speed in electrical radians per second and

$$\omega_r = P \omega_m \tag{5.1}$$

$\theta_r$ is the rotor position in electrical radians and

$$\theta_r = \int_0^t \omega_r dt \tag{5.2}$$

The value of back emf is dependent to both rotor position and rotor speed. It is assumed that the wave of back emf is changed sinusoidal.

$$\begin{bmatrix} e_a \\ e_b \\ e_c \end{bmatrix} = \frac{\omega_r K_T}{P} \begin{bmatrix} \sin \theta_r \\ \sin(\theta_r - \frac{2\pi}{3}) \\ \sin(\theta_r + \frac{2\pi}{3}) \end{bmatrix} \tag{5.3}$$

where $K_T$ is torque constant.

The parameters of BLDC are calculated in Chapter Three before;

$V_i = 4.6$ V,

$R = 0.167 \ \Omega$,

$L-M = 210 \ \mu H$,

$K_T = 0.03$ V/rad/sec,

$P = 4$,

$J = 0.000183$ kg.m$^2$.

$T_{f+w} = 0,0137$ Nm

$T_{f+w}$ is the friction and windage torque and it is calculated, when the motor is run at no-load.

BLDC motor is used to run a cooling fan and load torque is represented by the following equation,

$$T_L = \frac{0.0331}{349^2} \times \omega_r^2 \tag{5.4}$$

which is calculated by using actual BLDC motor with load. The load torque of cooling fans is generally related with square of rotor speed.

By using the direct back emf detection the correct commutation sequence is selected. Switching sequence is given below and the logic circuit for the mosfet gating signals is given in Figure 5.2 and Figure 5.3 (Pillay, P., et al., 1991).
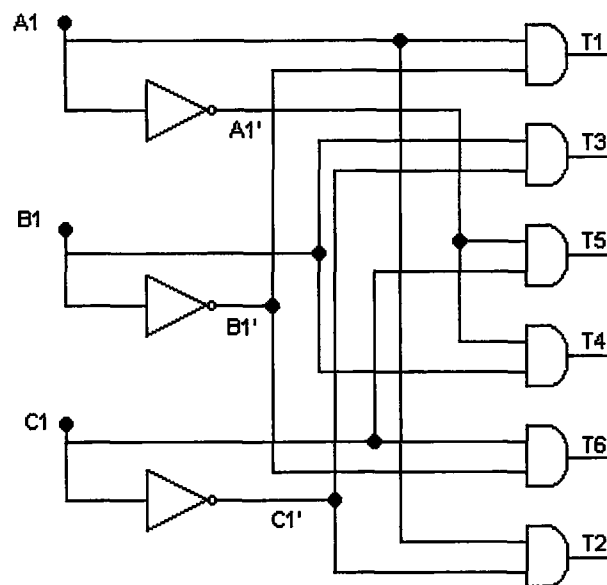
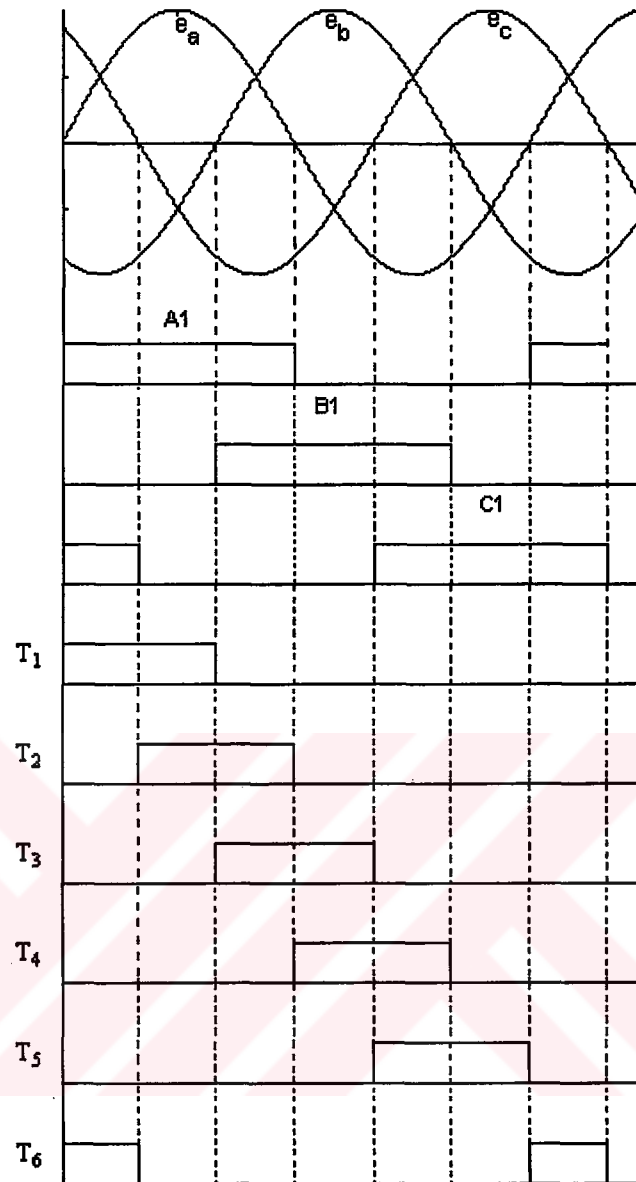$T1 = A1 \times B1'$

$T3 = B1 \times C1'$

$T5 = C1 \times A1'$

$T4 = B1 \times A1'$

$T6 = C1 \times B1'$

$T2 = A1 \times C1'$



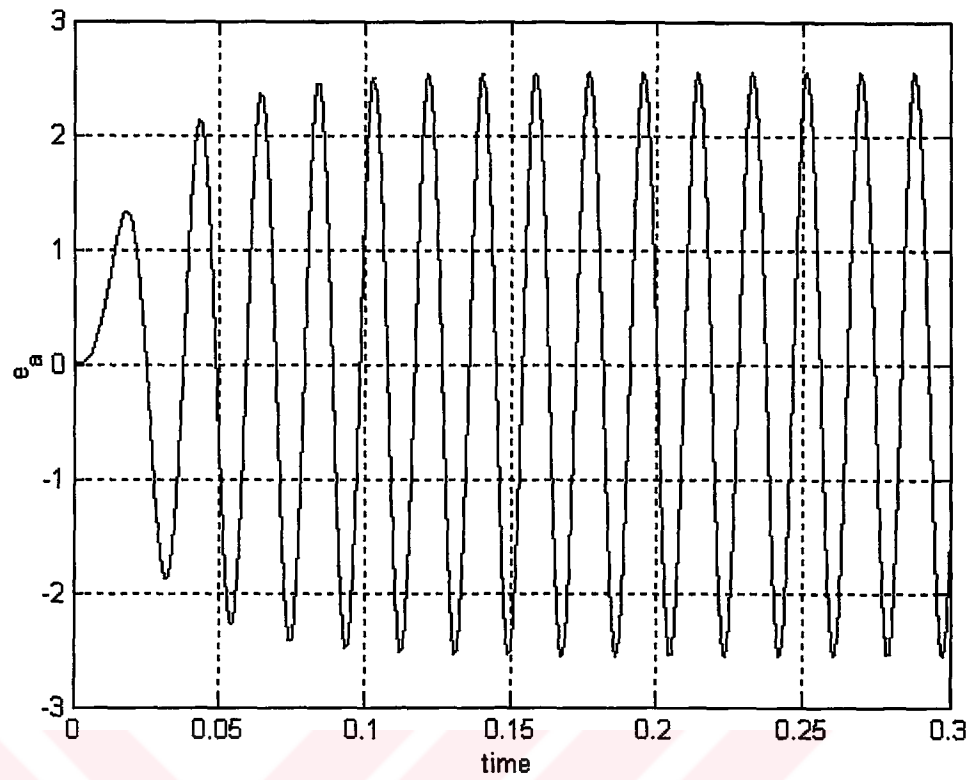**Figure 5.2 Logic circuit for the mosfet gating signals**

**Figure 5.3 Mosfet gating signals**

By using the logic circuit in Figure 5.2, the simulation results are given below,

**Figure 5.4 Back emf of phase a**
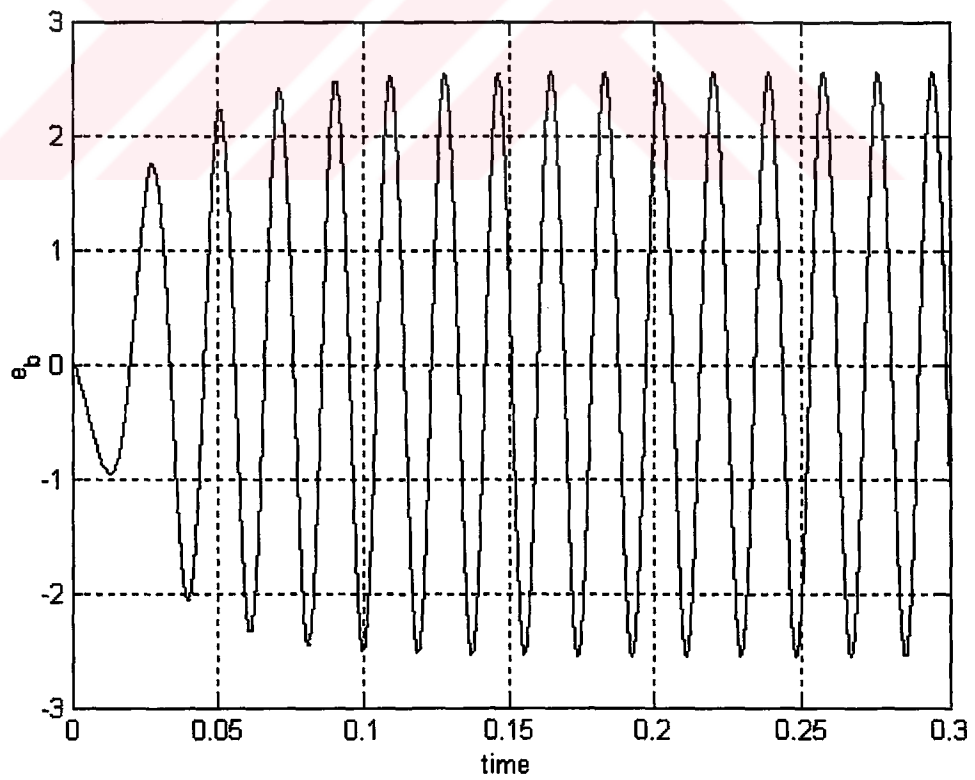


**Figure 5.5 Back emf of phase b**
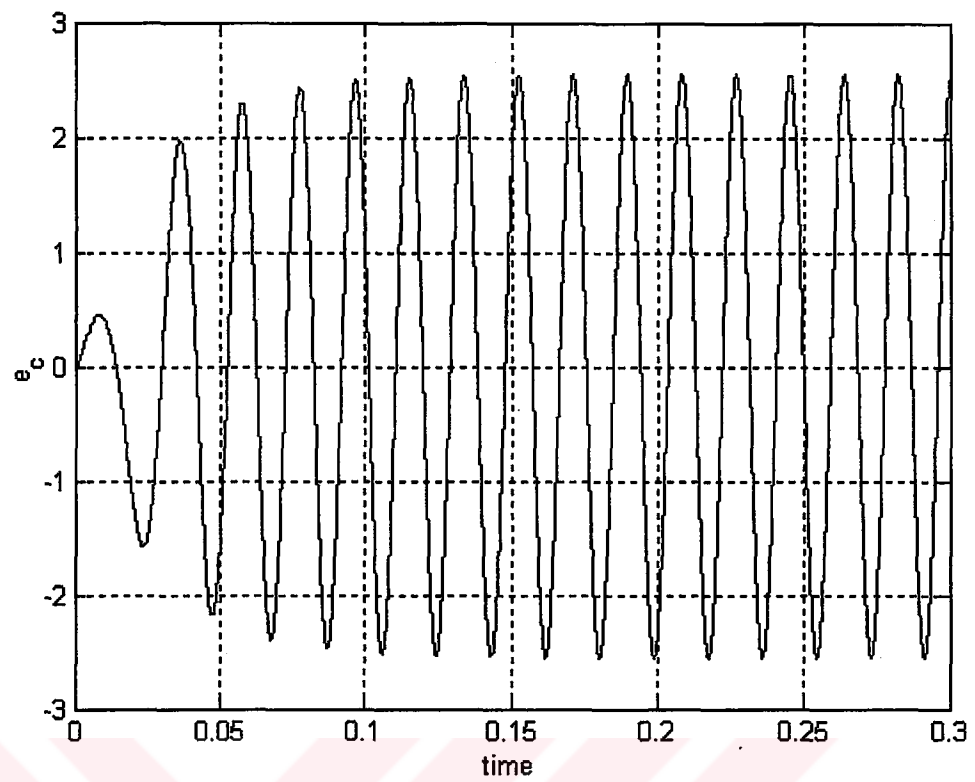
**Figure 5.6 Back emf of phase c**
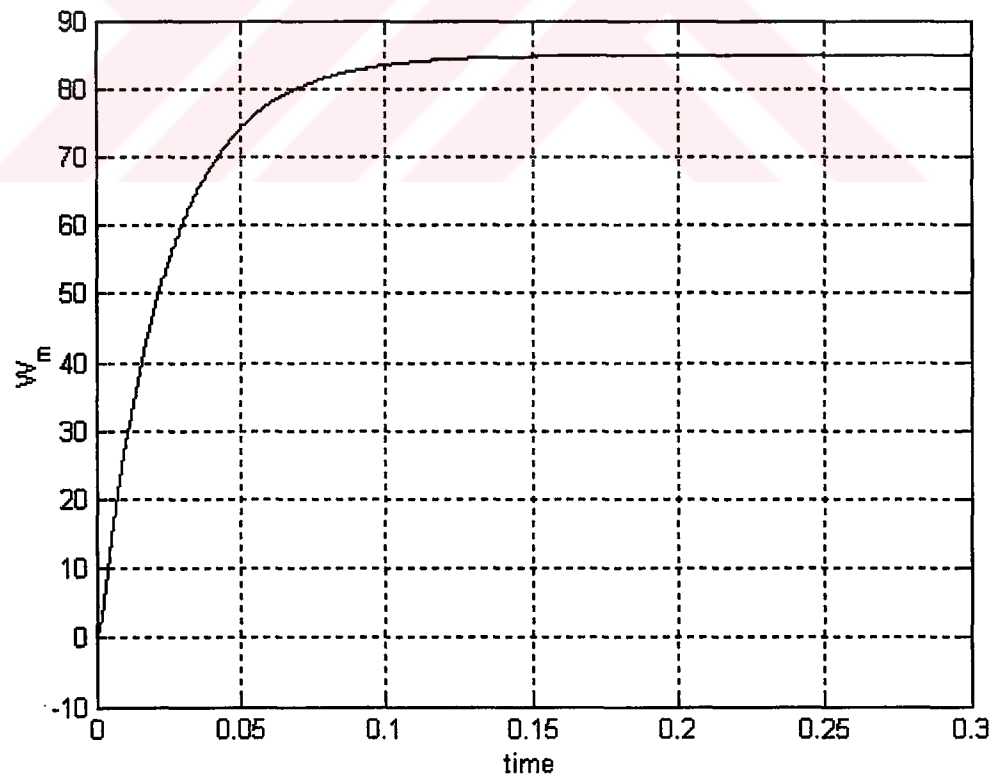


**Figure 5.7 Mechanical rotor speed**

**Figure 5.8 Current of phase a**
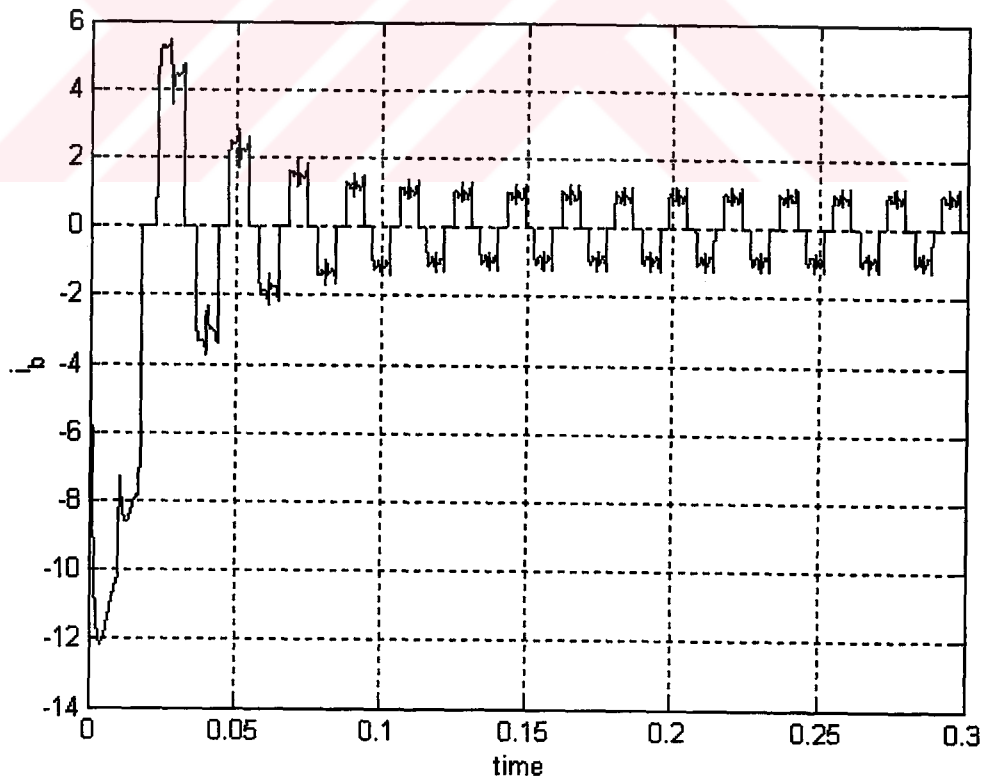


**Figure 5.9 Current of phase b**
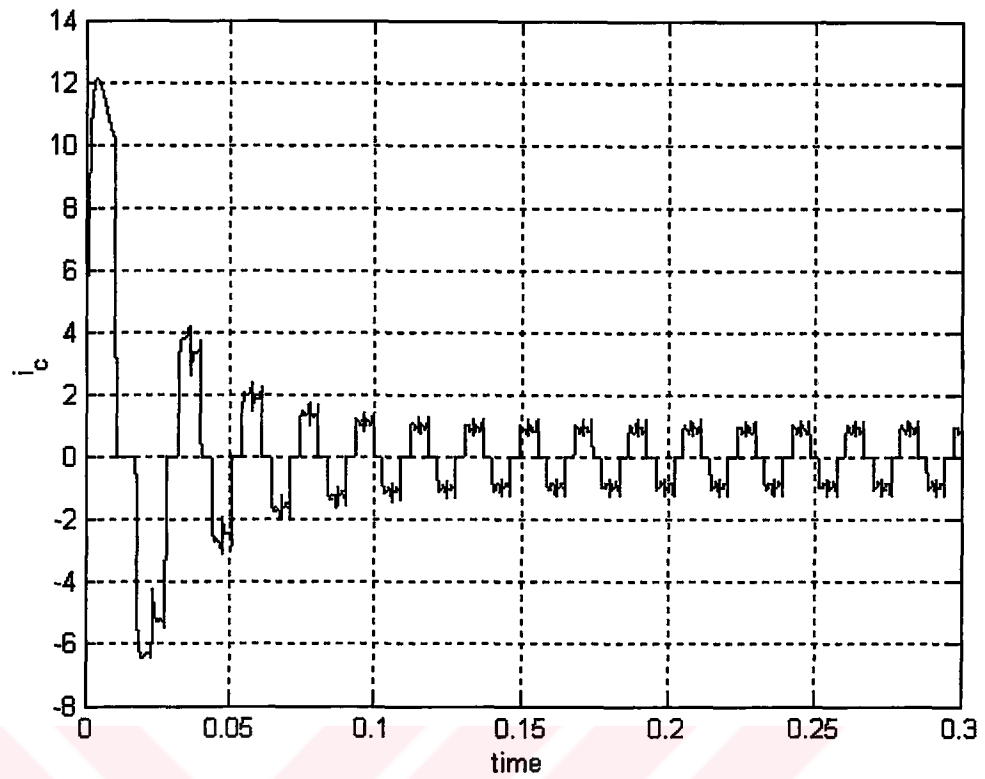
**Figure 5.10 Current of phase c**
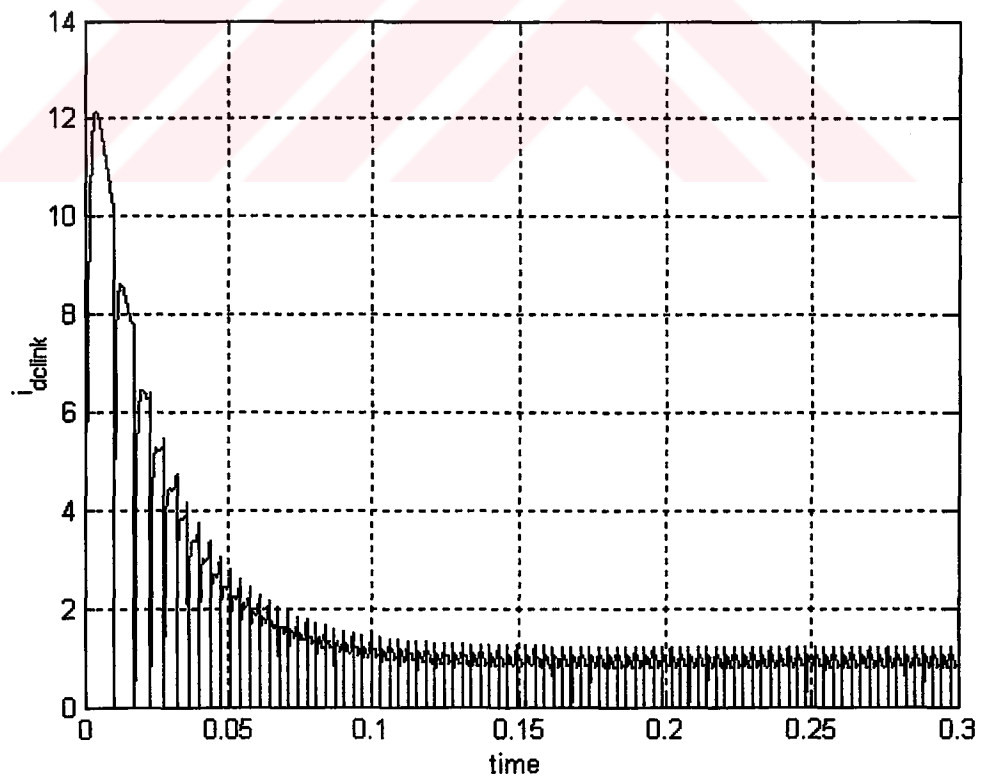


**Figure 5.11 DC link current**
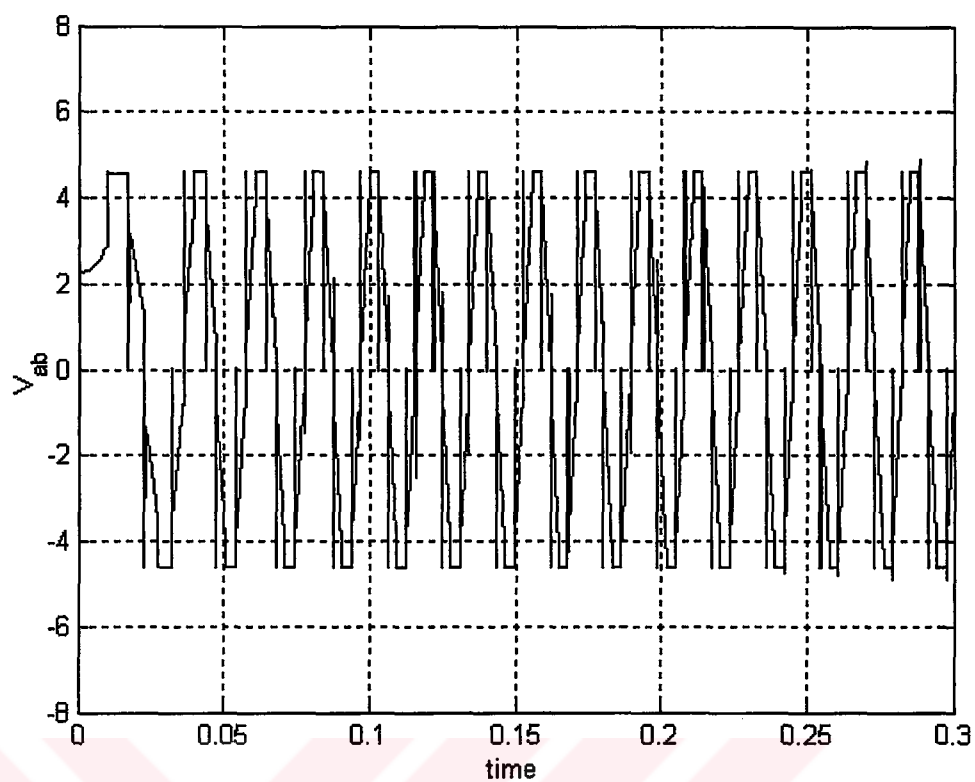
**Figure 5.12 Line-to-line voltage of phase a and phase b**
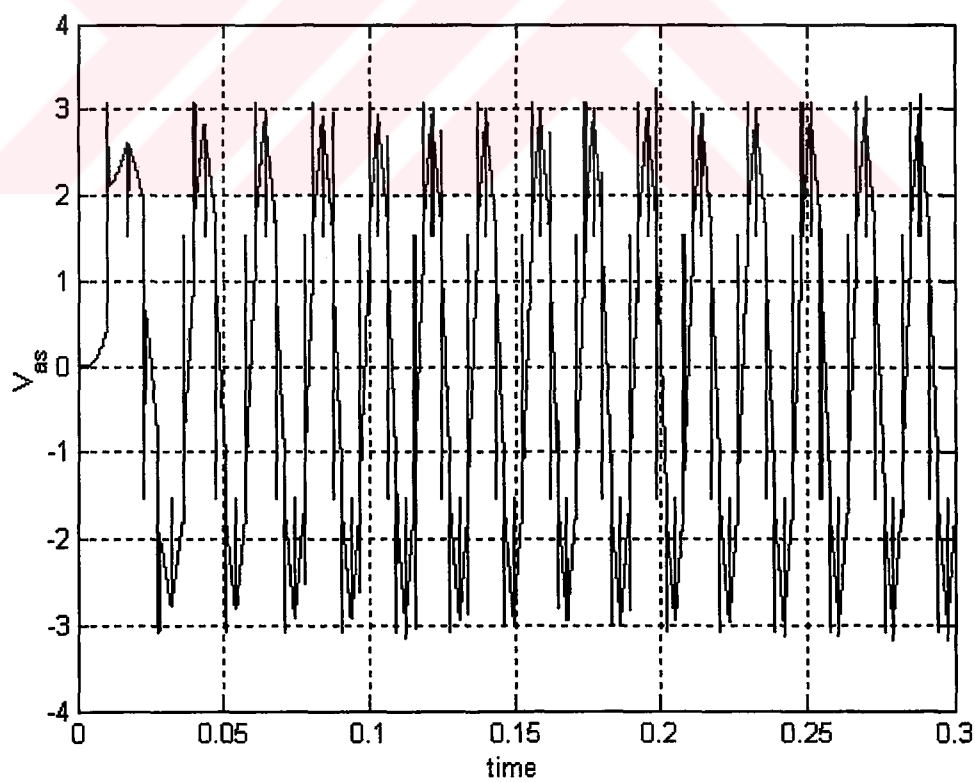


**Figure 5.13 Voltage of phase a**
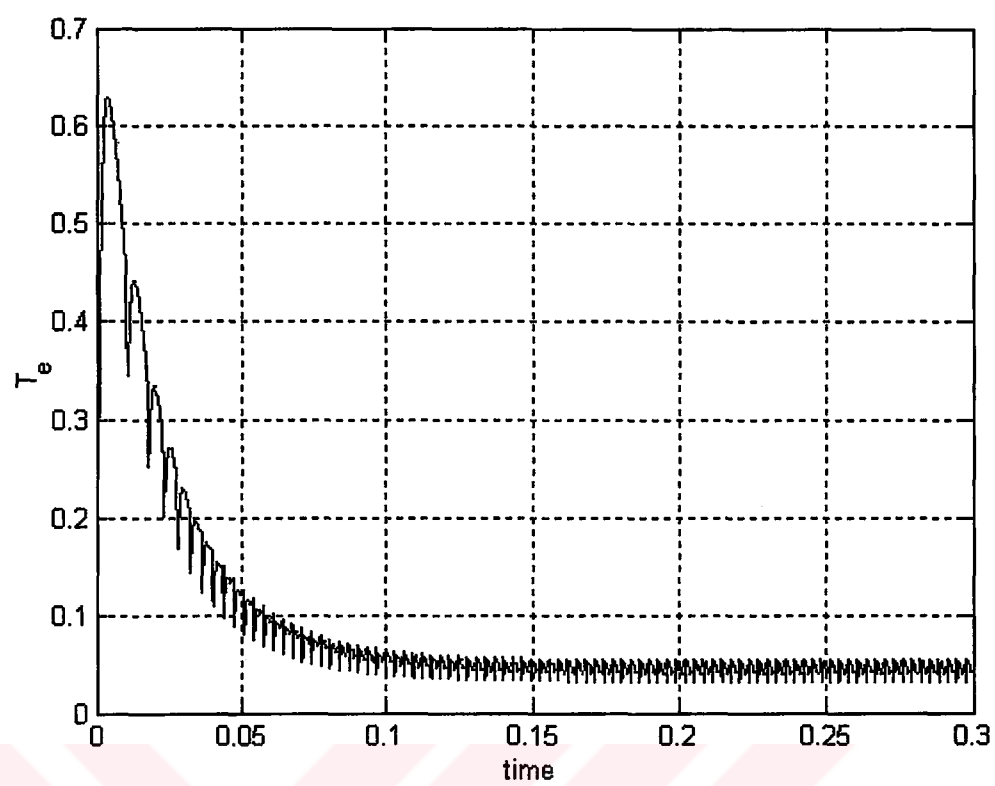
**Figure 5.14 Electromagnetic torque**
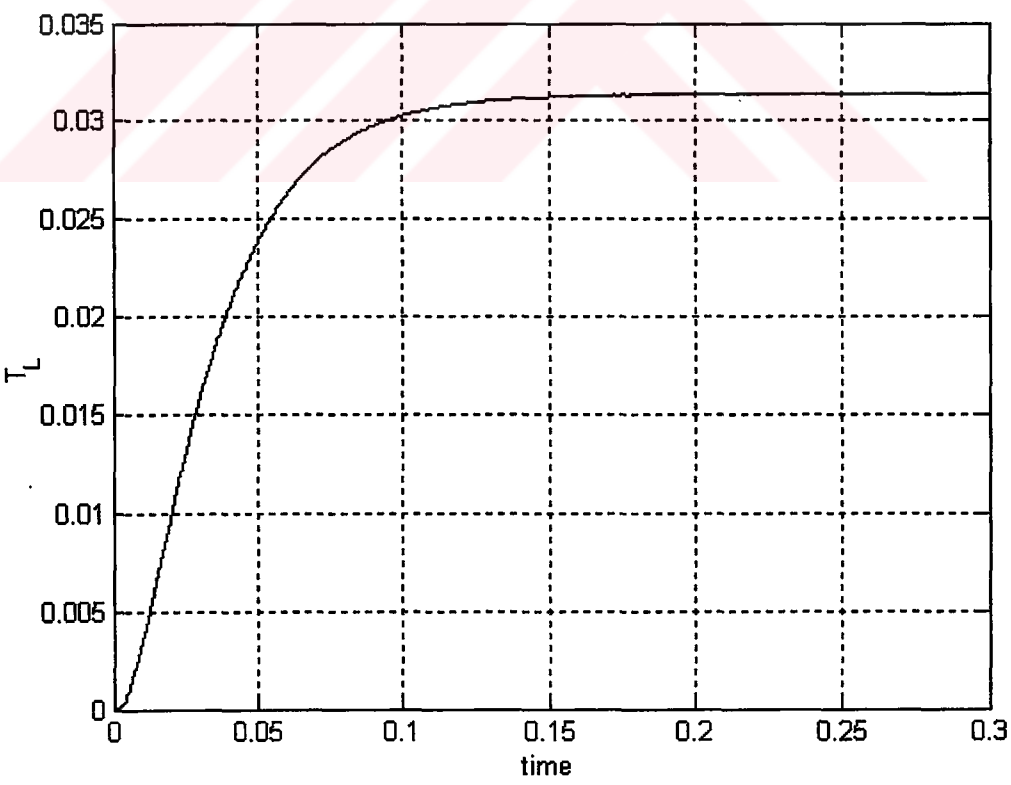


**Figure 5.15 Load torque**

When BLDC motor runs at the steady state speed, electromagnetic torque is equal to sum of the friction and windage torque and the load torque. The frequency of DC link current is six times greater than a phase current, as shown in Figure 5.16.
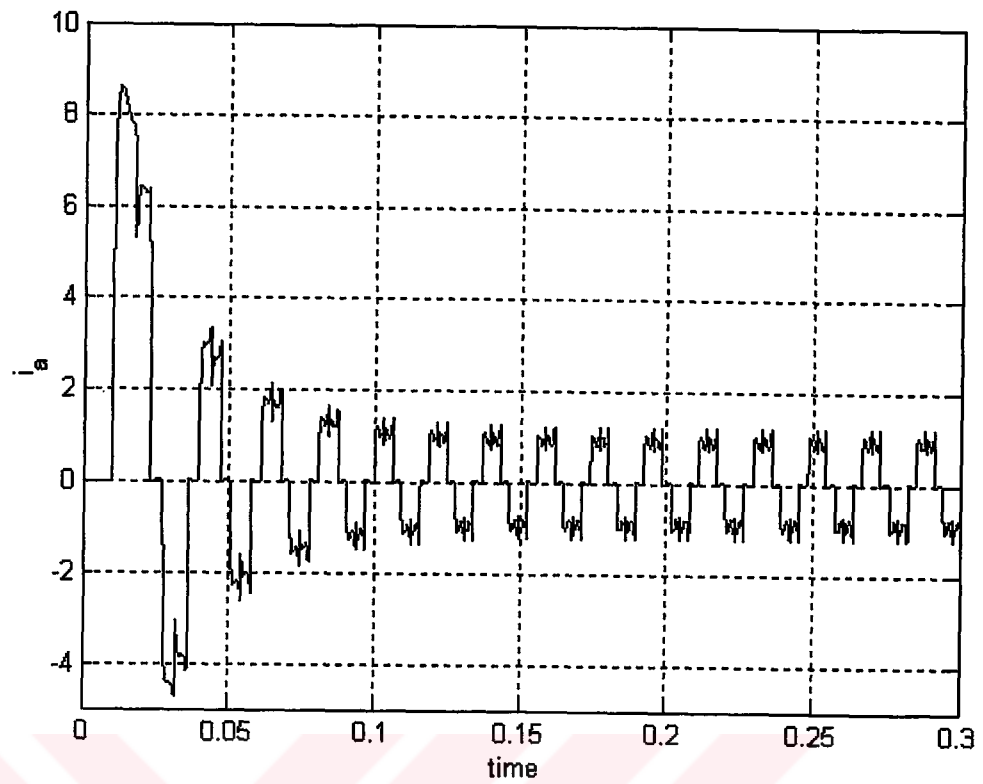


**Figure 5.16 DC link current and current of phase a**

As it is explained before, when the current of one of the phases is zero, the phase voltage is equal to back emf, it is clearly seen in Figure 5.17.

In normal condition back emf and current of the same phase are in phase, in order maximize the motor efficiency. The voltage and current waveforms of phase a are given in Figure 5.17.
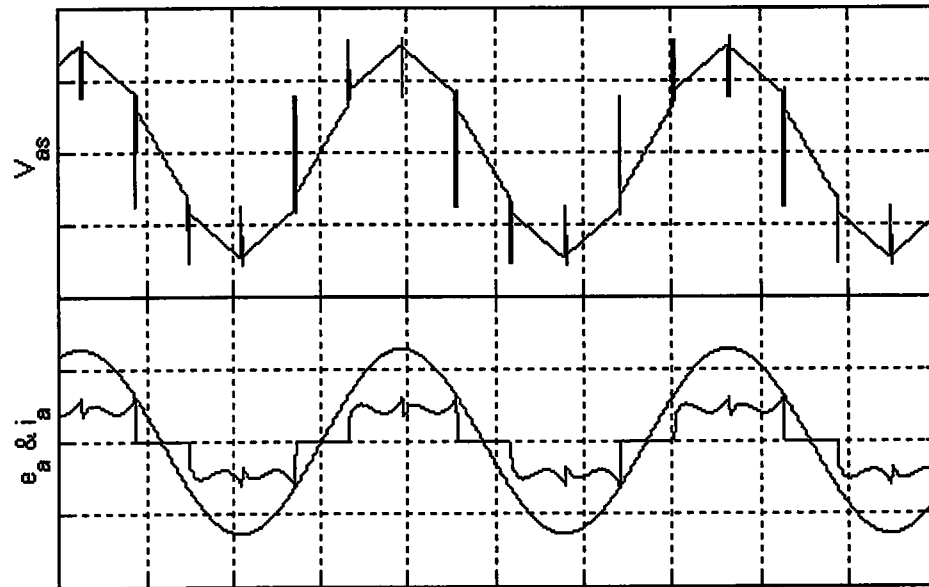
**Figure 5.17 Voltage, back emf, current of phase a**

## 5.2 Experimental Results of BLDC Motor

8 poles BLDC motor is connected TDA5142T Brushless DC Motor Drive Circuit of Philips. The features of TDA5142T are explained in Chapter Four. DC link voltage, $V_i$ is equal to 4.6 V.

The experimental results is given below
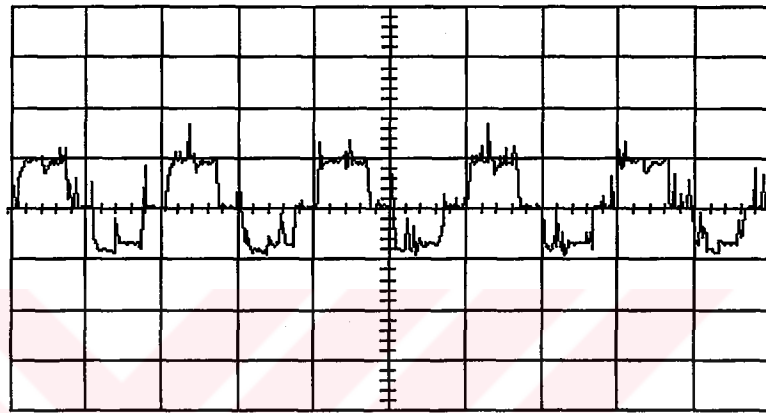


**Figure 5.18 Current of phase a (1 A/div, 10 msec/div)**
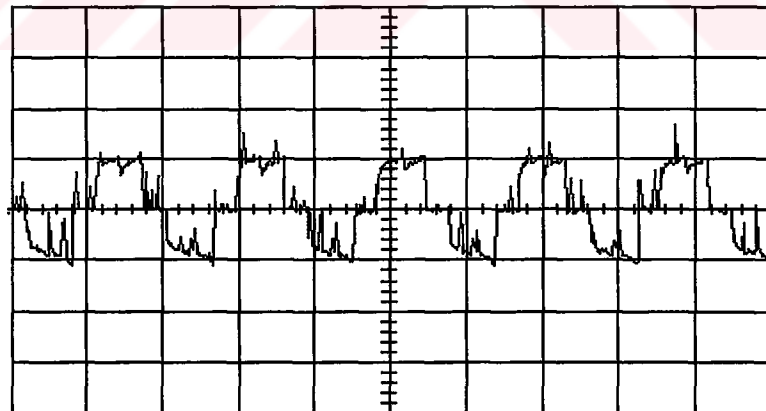


**Figure 5.19 Current of phase b (1 A/div, 10 msec/div)**
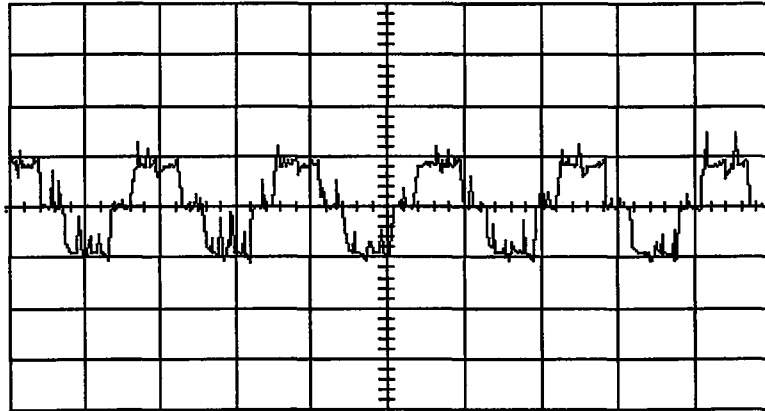
**Figure 5.20 Current of phase c (1 A/div, 10 msec/div)**
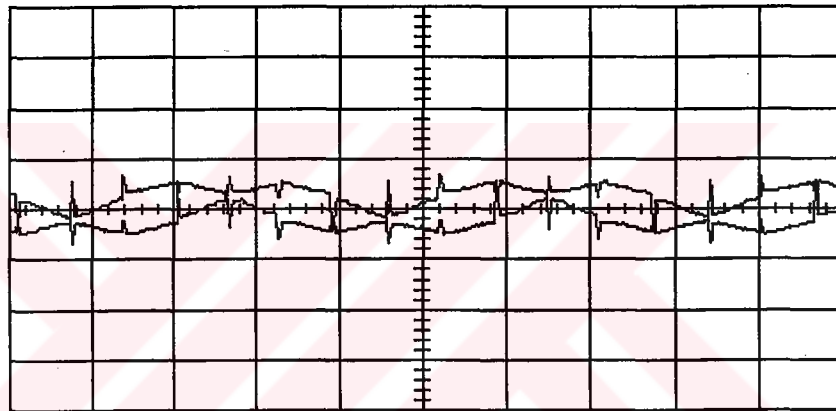


**Figure 5.21 Back emf of phase a and phase b (5 V/div, 5 msec/div)**
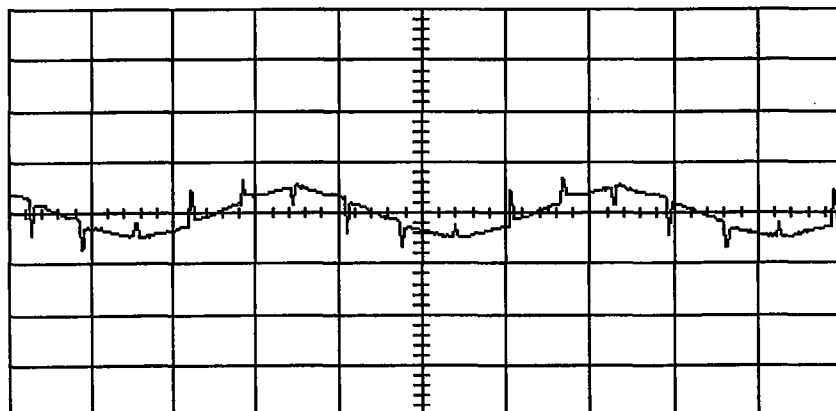


**Figure 5.22 Back emf of phase c (5 V/div, 5 msec/div)**
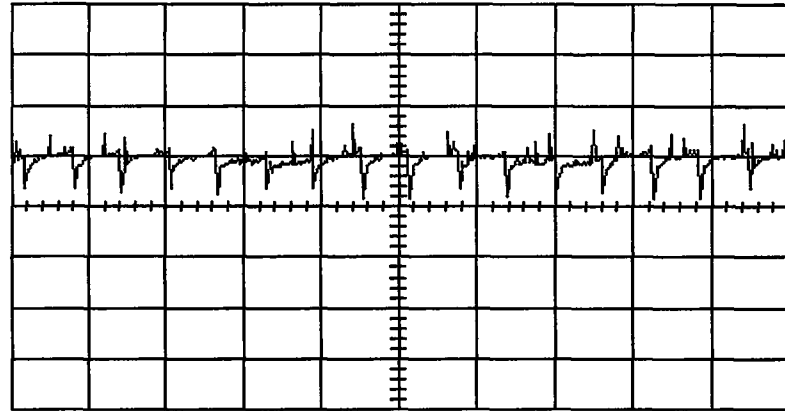
**Figure 5.23 DC link current (1 A/div, 5 msec/div)**

As in the computer simulation frequency of the DC link current is equal to six times of a phase current, shown in Figure 5.24,
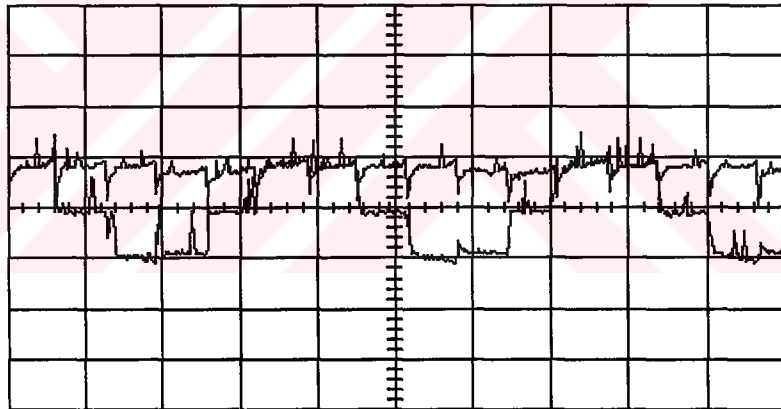


**Figure 5.24 DC link current and current of phase a (1 A/div, 5 msec/div)**
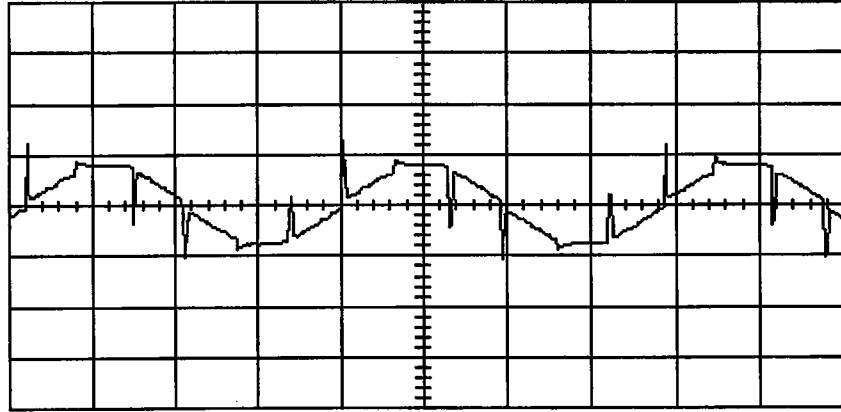
**Figure 5.25 Line-to-line voltage of phase a and phase b (5 V/div, 5 msec/div)**

## 5.3 Comparison of Results

When the predicted steady state current of phase obtained from computer simulation shown in Figure 5.26 is compared to the measured current of phase a, shown in Figure 5.18, the amplitude and frequency of both waveforms are equal but it is seen that there are some more spikes on the actual current.



**Figure 5.26 Steady state current of phase a using computer simulation (1 A/div, 10 msec/div)**

In implementation the phase voltages are detected to supply the commutation sequence, but in computer simulation sinusoidal variation of back emfs are used as a reference for the commutation. The steady state voltage of phase a obtained from simulation, shown in Figure 5.27 is similar to the actual voltage of phase a, shown in Figure 5.21. The dc link current and line-to-line voltages from simulation are given in Figure 28 and 29 respectively, when these waveforms are compared to the experimental results given in Figure 5.23 and 5.25, it is observed that the simulation program predicts the actual waveform quite well.

Since the saturation and nonlinearity are not included into the model, the solution obtained from the computer simulation is not exact solution, but computer simulation and experimental results are compared, the computer simulation gives satisfactory results.
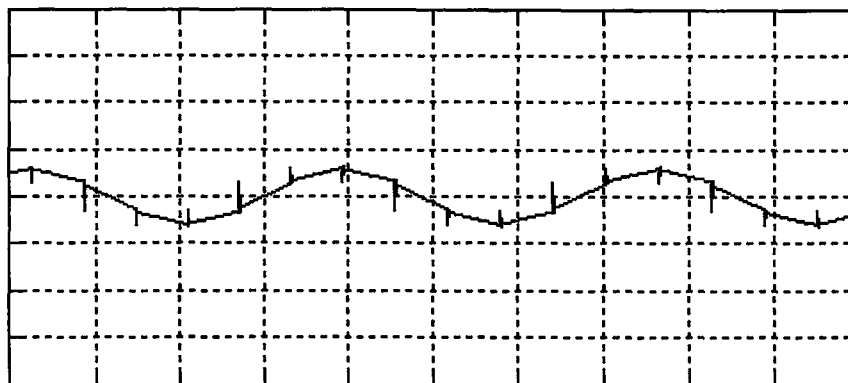
**Figure 5.27 Steady state back emf of phase a using computer simulation**

**(5 V/div, 5 msec/div)**



**Figure 5.28 Steady state DC link current using computer simulation**

**(1 A/div, 5 msec/div)**
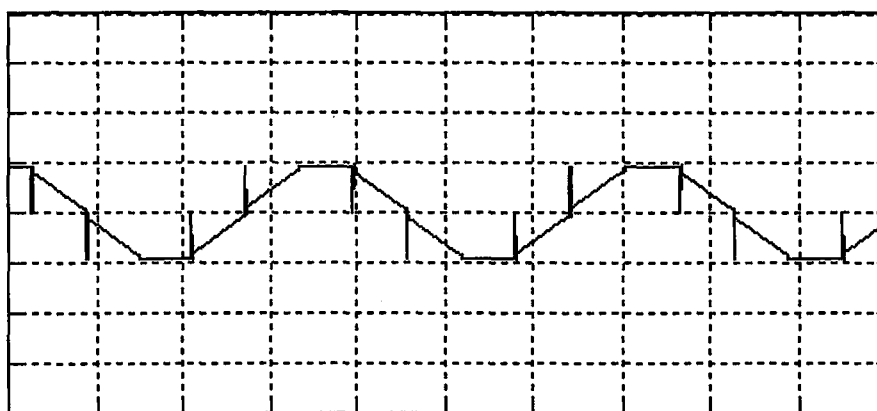


**Figure 5.29 Steady state line-to-line voltage using computer simulation**

**(5 V/div, 5 msec/div)**

The efficiency of the entire system is

$$\%\eta = \frac{T_L \omega_m}{V_i I_i} \times 100.$$

(5.5)

In the computer simulation program,

$V_i = 4.6$ V,

$I_i = 0.9$ A, which is the DC component of the DC link current and it is determined by using Fourier Transform,

$\omega_m = 85$ rad / sec, which is the steady state speed of BLDC motor,

$T_L = 0.0314$ Nm, which is calculated from equation (5.4).

$$\%\eta = \frac{85 \times 0.0314}{4.6 \times 0.9} \times 100 = 65\%$$

(5.6)

In the actual system,

$V_i = 4.6$ V,

$I_i = 0.85$ A, which is red from dc supply,

Rotor speed is measured with tachometer or determined from the frequency of a phase current, frequency of phase current is calculated from Figure 5.18, frequency f is equal to 52.63 Hz, then by using ($2\pi f$) the rotor angular speed in electrical radians per second is found, the electrical rotor speed $\omega_r$ is equal to 330.69 rad / sec. From equation (5.1), the mechanical rotor speed is calculated

$$\omega_m = \frac{\omega_r}{P} = \frac{330.69}{4} = 82.7 \text{ rad / sec.}$$

(5.7)

And load torque is calculated by using equation (5.4),

$T_L = 0,03$ Nm.

$$\%\eta = \frac{82.7 \times 0.03}{4.6 \times 0.85} \times 100 = 63\%$$

(5.8)

## 5.4 BLDC Drive System

Motor control system consists of a position controller, a speed controller, and a current (torque) controller. If only speed control is desired, the position controller is discarded. The block diagram of the drive system is shown in Figure 5.30.
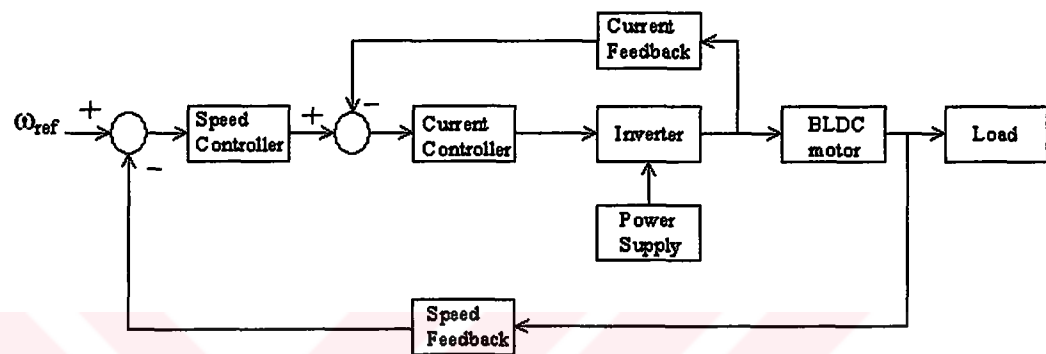


**Figure 5.30 Block diagram of the drive system**

It is clear that the frequency of the voltages applied to the machine is determined by the switching frequency of the inverter. As the frequency of the applied voltages is reduced it is necessary to reduce the value of the applied machine voltages. The effective value of the phase voltages is generally reduced by a process referred to as pulse width modulation (PWM). In the case of the PWM inverter the phase voltages are periodically stepped to zero during a cycle whereby the average value of the output voltage may be controlled. Hence the speed is also controlled.

There are many current control techniques, for example; hysteresis current control, ramp comparison control, predictive control, delta current control, complex space vector-current control, sliding mode current control, etc.

Hysteresis current control is most extensively used method. It responds quickly, requires no load information, and is easy to implement. However, hysteresis current controllers have several disadvantages. The steady state current ripples are relatively high. Switching frequencies vary during operation, leading to irregular inverter operation and generating PWM noise. This control is examined in (Pillay, P. & Krishnan, R., 1989) and its performance is compared with PWM current controller.

The main advantage of the ramp comparison technique is that the switches operate at fixed frequencies. However, problems include appreciable phase lags and magnitude errors at high frequencies, and complicated PLL circuits are required to overcome these problems.

Predictive control gives good performance in terms of response time and accuracy; it requires extensive calculation and accurate load information.

Sliding mode current control is one of the recently developed current control techniques. Broad bandwidth and robustness to parameter variation are among its advantages. Current control using the sliding mode technique was applied in (Chen, J., & Tang P., 1999). Further information about the current controller is given in (Wu, M., 1992).

## 5.5 Computer Simulation of Closed-Loop Control

This BLDC motor has trapezoidal back emfs. Therefore, the peak of sinusoidal waveform has been cut off in order to get similar shape to trapezoidal waveform in the model used in Matlab.

The parameters of motor are given below;

R = 0.107 Ω,

L-M = 0.34 mH,

$\lambda_m$ = 0.01423 V / rad / sec,

P = 2,

J = 0.000183 kg m$^2$,

$$T_L = \frac{0.365}{564^2} \times \omega_r^2,$$

(5.9)

$P_{f+w}$ = 13 W, where $P_{f+w}$ is the friction and windage loss.

The BLDC motor has been fed by 3-phase six-step bridge inverter having 6 MOSFETs. The commutation strategies, drive conditions for maximum efficiency, and sensorless operation are discussed before. The block diagram of control circuit used in this work is given in Figure 5.31. The back emf detection consists of reading, at each step in the non-energized phase, the instant when the back emf crosses zero. The PWM is only applied to the high side MOSFETs for the detection of the zero crossing events. The control principal of simulation is to obtain maximum efficiency from the motor by keeping the phase current in phase with the back emf in the same winding. The phase current is limited to 20 A at the starting.
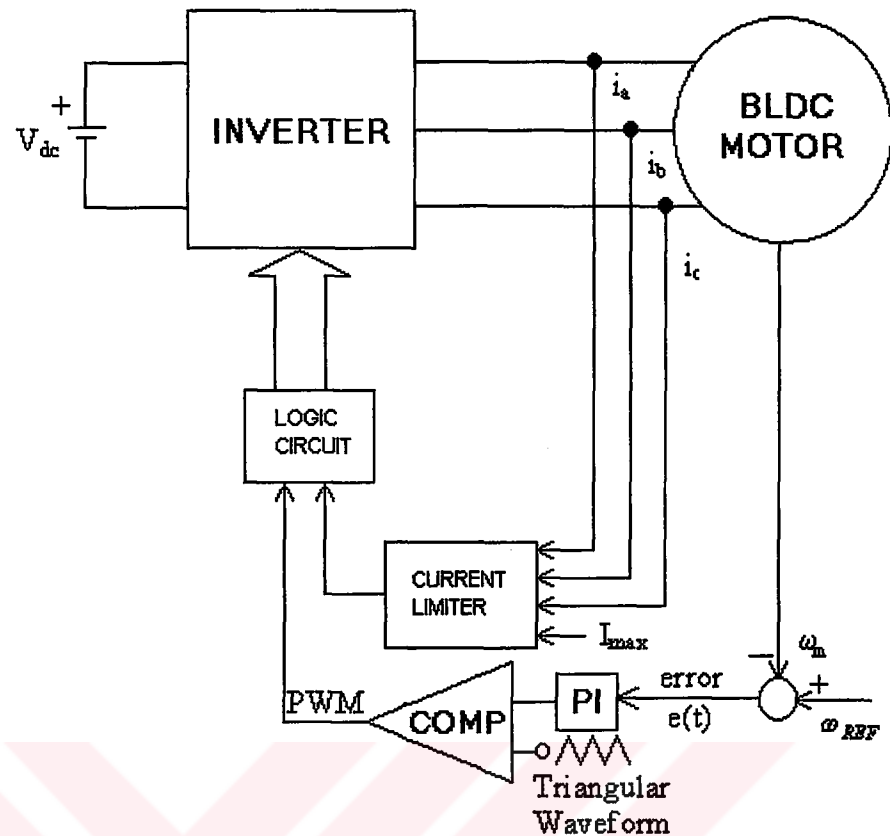
**Figure 5.31 Control strategy for BLDC**

### 5.5.1 Design of a PID Controller

PID control is proportional-integral-derivative control, which consists of a proportional gain, an integral gain, and a derivative gain. The proportional term controls the loop gain of the system and therefore reduces system sensitivity to parameter variations. The integral term increases the order of the system in order to reduce the steady state error. The derivative term helps to stabilize the system. The selection of the coefficients or gains associated with these three terms is called tuning. It is often done by using an established design method to get a starting point, followed by an intuitive trial-and error method.

There are many methods for tuning a PID controller, varying in complexity from simple rules based on open loop response to self-tuning algorithms. One of the better-known techniques is the Ziegler-Nichols step response method.

In this method, a step response of the open-loop system is recorded. An example is shown in Figure 5.32. Two parameters are taken from this response-the maximum gradient, A, and the point at which this line of maximum gradient crosses the time axis, B. The magnitude of the input step is taken to be $U$. The three gains for a full PID controller are calculated using
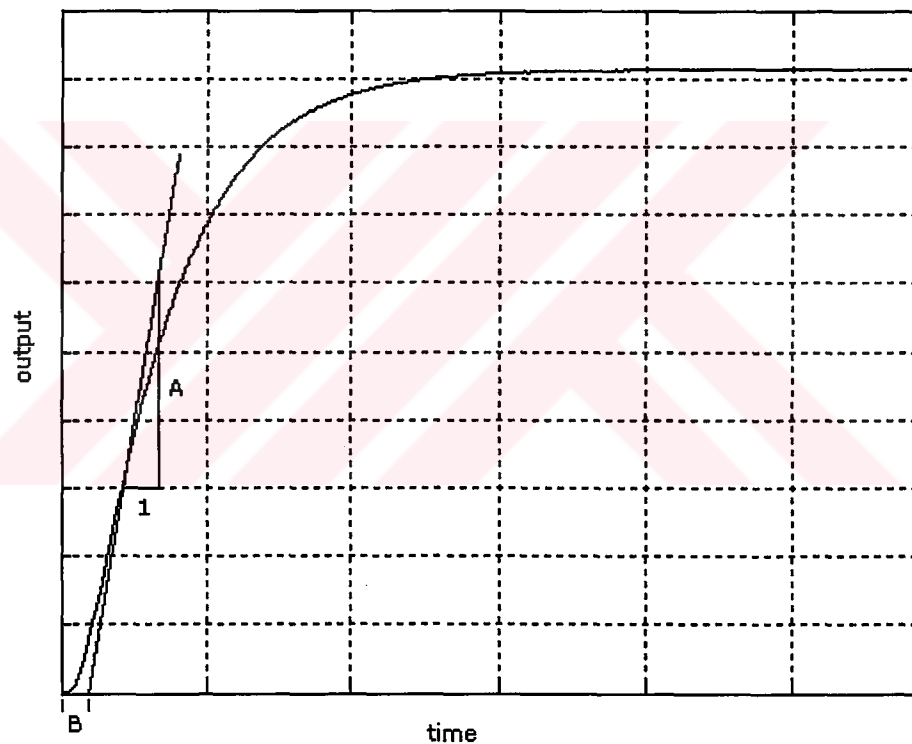


**Figure 5.32 Step response of third-order system showing Ziegler-Nichols PID design technique**

$$k_c = 1.2 \frac{U}{AB} \tag{5.10}$$

$$T_i = 2B \tag{5.11}$$

$$T_d = 0.5B \tag{5.12}$$

where the PID controller is represented by

$$C(S) = k_c (1 + 1 / T_i s + T_d s) \tag{5.13}$$

The engineer would implement the controller with these gains and then "adjust on test" to achieve a satisfactory closed-loop response (Hendershot, J.R. & Miller, T.J.E., 1994).

For simulation program the proportional coefficient, $k_p$ and the integral coefficient, $k_i$ are determined by using this method, then adjusting these coefficients the most suitable values are found. For this system, $k_p = 200$, $k_i = 17$.

### 5.5.2 Results of Computer Simulation

$V_i$ is equal to 26 V, the frequency of the triangular signal is 6 kHz, reference speed, $\omega_{REF}$ is 282 rad/sec. In this simulation program $0°$, $30°$, and $60°$ phase delay are given to the mosfet gating signals, to compare efficiencies. The phase delays between back emfs and phase currents are seen clearly in Figure 5.33, Figure 5.34 and Figure 5.35. The efficiencies are calculated for each delay angle in Table 5.1.

**Table 5.1 Efficiencies according to the delay angles.**

| Delay Angle | $V_i$ | $I_i$ | $T_L$ | $\omega_m$ | $\eta$ % |
|---|---|---|---|---|---|
| 0° | 26 V | 5.8 A | 0.365 Nm | 282 rad/sec | 68 |
| 30° | 26 V | 5.6 A | 0.365 Nm | 282 rad/sec | 71 |
| 60° | 26 V | 6.5 A | 0.365 Nm | 282 rad/sec | 61 |
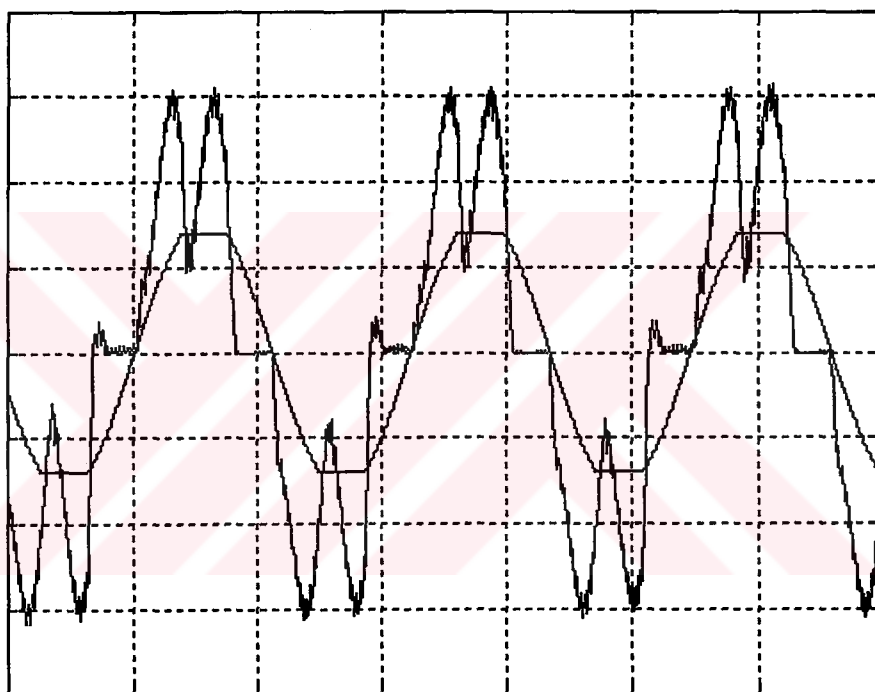


**Figure 5.33 No-phase delay between back emf and phase current**
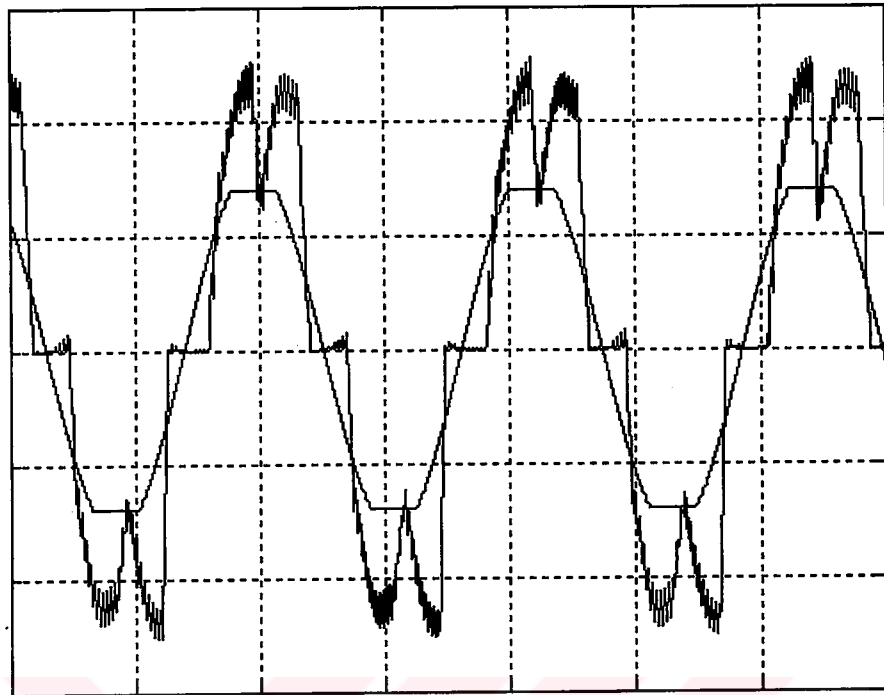
**Figure 5.34 30° phase delay between back emf and phase current**
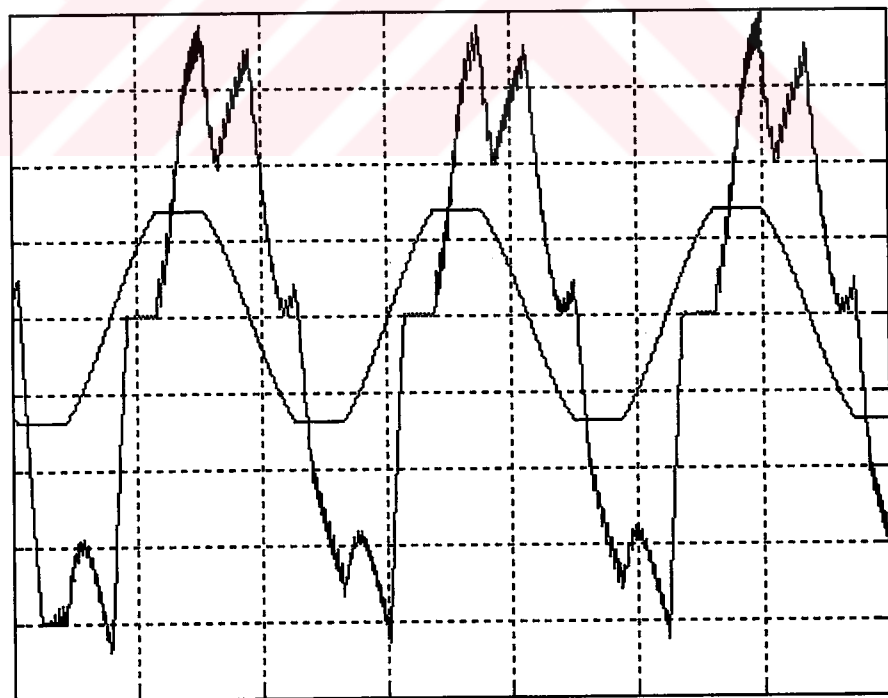


**Figure 5.35 60° phase delay between back emf and phase current**

For $30^\circ$ delay angle, the motor efficiency is maximum. Therefore, it is assumed that the motor is driven by the inverter to keep maximum efficiency and the rest of the results are obtained with these gating signals.
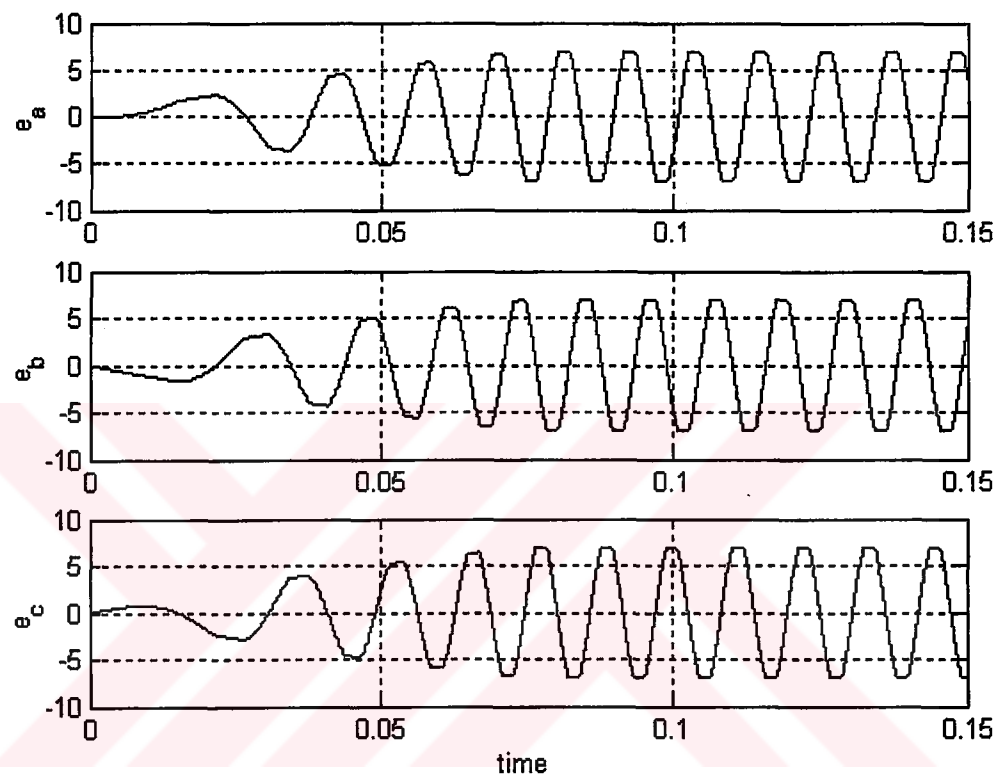


**Figure 5.36 Back emfs of BLDC**
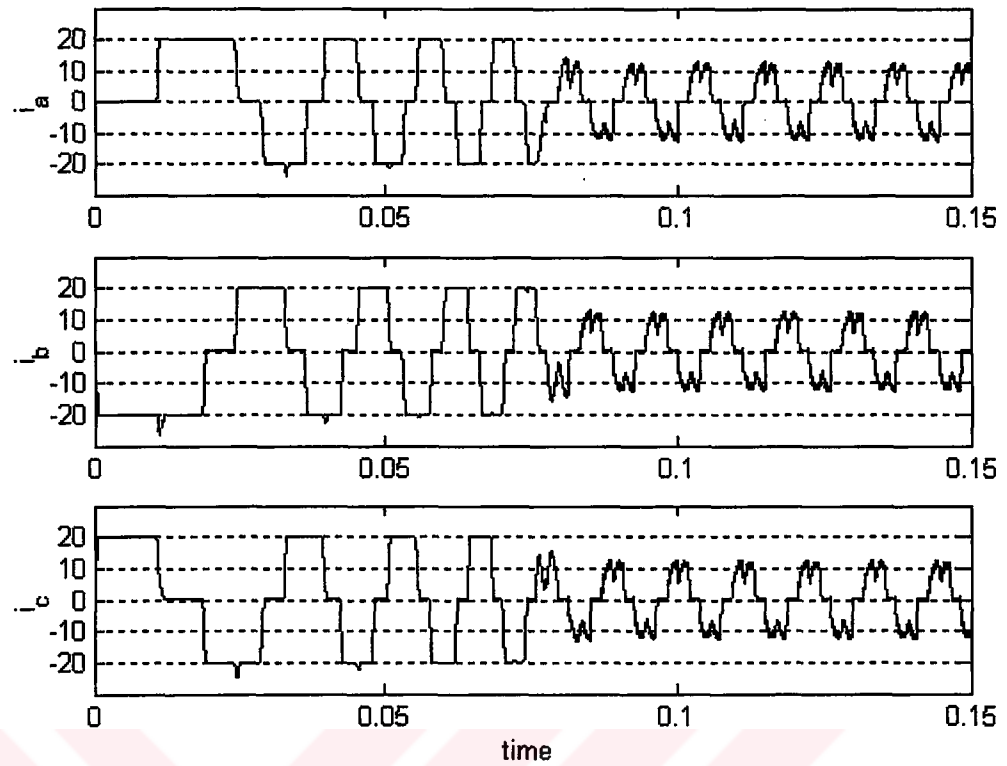
**Figure 5.37 Phase currents**
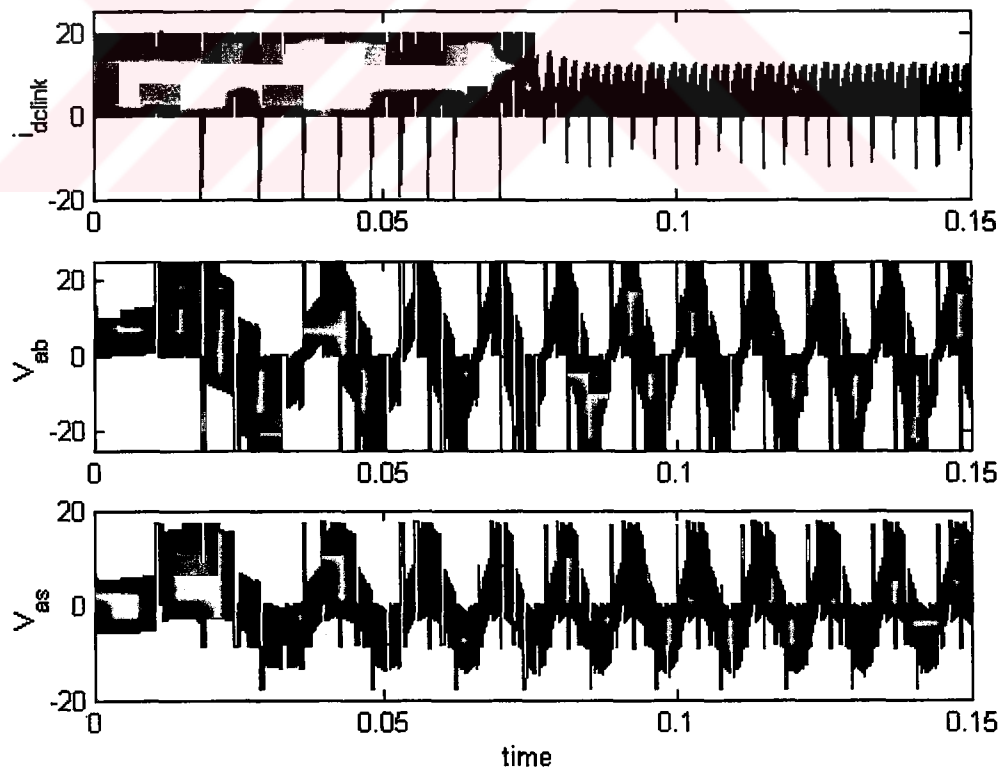


**Figure 5.38 DC link current, line-to-line voltage, and phase voltage**
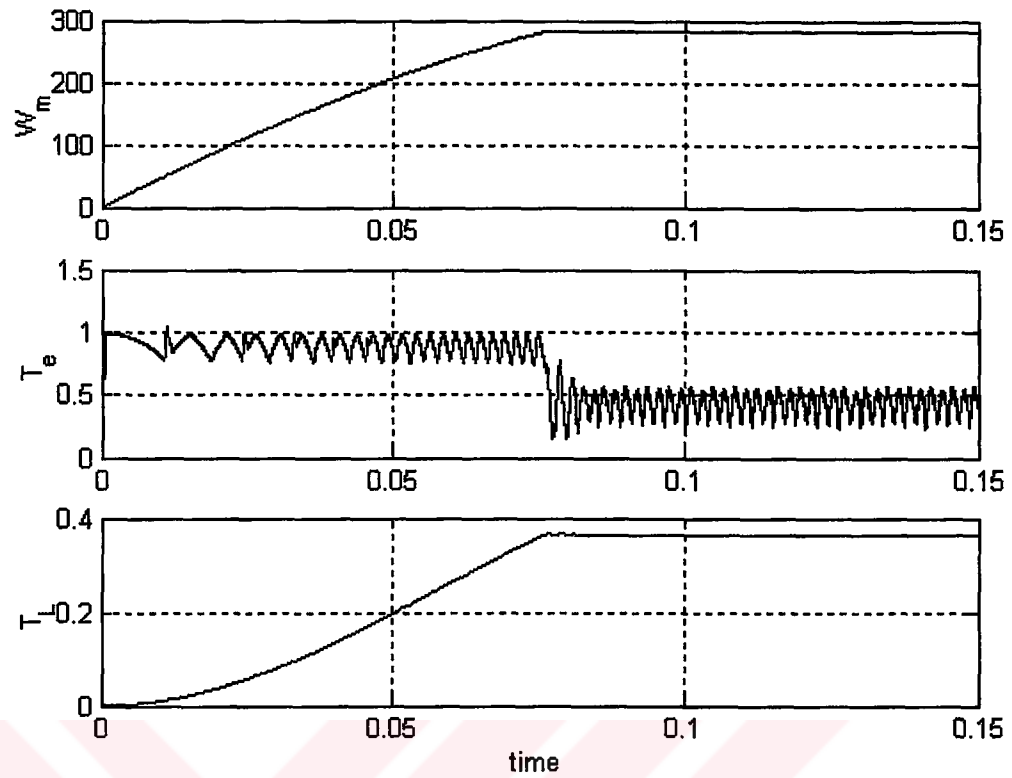
**Figure 5.39 Mechanical rotor speed, electromagnetic torque, load torque**
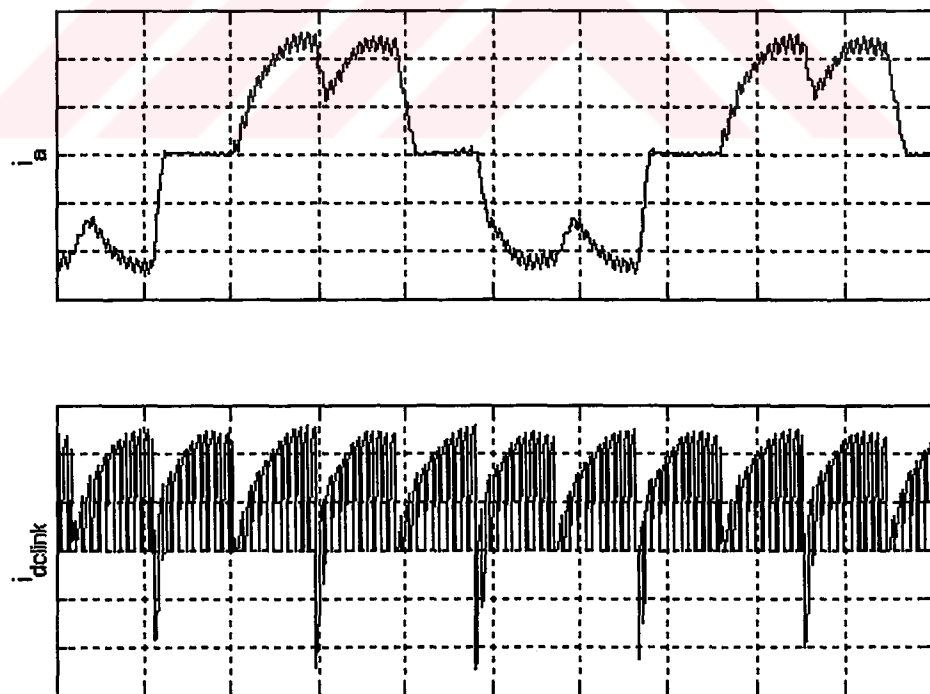


**Figure 5.40 Current of phase a and DC link current**

PI control gives sufficient performance; the steady state speed has less than 0.1% error. It is shown that the PI coefficients are very good adjusted.

---

# CHAPTER SIX

# CONCLUSIONS

---

In this thesis, a BLDC motor and its drive circuit are analyzed. Then a drive circuit is designed and implemented in laboratory. Computer simulation program is prepared in the MATLAB Simulink using mathematical model of BLDC motor. The experimental circuit is implemented using TDA5142T brushless dc motor drive circuit of Philips. The reason of selecting this integrated circuit is that, this circuit has a low cost and simple structure

Computer simulation program has 2 blocks, one is the BLDC motor block and the other is gating signal block for commutation sequence. In the BLDC motor block, it is assumed that the back emfs are sinusoidal. In the other block, mosfet gate signals are formed using the zero-crossings of the back emfs.

TDA5142T provides a good solution for the BLDC motor drive, if the motor does not have high load torque, (for example: Computer peripherals, printers...etc.). The gate signals of the inverter are supplied by TDA5142T, which operates at the $120°$ conduction mode. In this mode two phases are active, third phase is open. The commutation logic for the gate signals is provided using the EMF comparator. The back EMF is measured at this third phase. The zero-crossing in the back EMF is detected by the comparator, and this zero-crossing is used to calculate the correct moment for the next commutation. The speed control is made varying the dc supply voltage.

In this thesis, another BLDC motor and its closed loop control are simulated in Matlab. This motor has trapezoidal back emfs. The PI control is used to control rotor speed, the suitable parameters of PI are adjusted and PWM is used as a current controller. Moreover a current limiter is also used in order to protect motor and power components against the over current.

This motor and its drive is analyzed for the $0°$, $30°$, $60°$ phase delays. For $30°$ phase delay, the efficiency is higher than others, because the current reaches the peak value at the same time with the maximum value of back EMF.

BLDC motors compete with many other types of motors in the world of motion control. BLDC motor technology has been recognized as superior. In many applications, the improved feature-set justifies a significant cost difference. Fortunately for applications that cannot tolerate a cost differential, the price of BLDC is falling with the improvement of related technologies and with the extensive investment made in the manufacture of BLDC motors. As the costs of BLDC motors continue to fall, they will more often be the motor of choice.

# REFERENCES

Berendsen, C.S., & Champenois G., & Bolopion A., (1993). Commutation Strategies for Brushless Dc Motors: Influence on Instant Torque. IEEE Transactions on Power Electronics, Vol.8, No.2, pp. 231-236.

Bose, B.K., (1989). Applications Notes. IEEE Industry Applications Society Annual Meeting.

Chen, J., & Tang, P., (1999). A Sliding Mode Current Control Scheme for PWM Brushless Dc Motor Drives. IEEE Transactions on Power Electronics, Vol.14, No.3, pp. 541-550.

Ellis, G., (1996). Advances in Brushless DC Motor Technology, Control, and Manufacture. Kollmorgen Corporation, Radford, Virginia, USA.

Ertugrul, N., & Acarnley, P.P., (1998). Indirect Rotor Position Sensing in Real Time for Brushless Permanent Magnet Motor Drives. IEEE Transactions on Power Electronics, Vol.13, No.4, pp.608-616.

Hendershot, J.R., & Miller, T.J.E., (1994). Design of Brushless Permanent-Magnet Motors, Claredon Press-Oxford.

Kenyo, T., & Nagamori, S. (1985). The Permanent-Magnet and Brushless Dc Motors Clarendon Press Oxford.

Lee, E.C., Application of Brushless Dc Drives in Blow Molding. Powertec Industrial Corporation.

Miller, T.J.E. (1989). Brushless Permanent-Magnet and Reluctance Motor Drives Clarendon Press Oxford.

Nehl, T.W., & Demerdash N.A. (1992). Direct Current and Permanent Magnet Motors in Adjustable Speed Drives. IEEE Tutorial on Adjustable Speed Drives.

Ong, Chee-Mun. (1998). Dynamic Simulation of Electric Machinery Using Matlab Simulink. Prentice Hall PTR.

Park, S.J., & Park, H.W., & Lee, M.H., & Harashima, F. (2000). IEEE Transactions on Industrial Electronics, Vol.47, N0.1, pp.109-114

Pillay, P., & Krishnan, R. (1989). Modelling, Simulation, and Analysis of Permanent-Magnet Motor Drives, Part II: The Brushless Dc motor Drive. IEEE Transactions on Industry Applications, Vol.25, No.2, pp.274-279.

Pillay, P., & Bose, B.K., & Jahns, T.M., & Lorens, R.D., & Slemon, G.R., & Strnat, K. (1991). Performance an Design of Permanent Magnet AC Motor Drives, New York, USA.

Rashid, M.H. (1993). Power Electronics Circuits, Devices, and Applications (Second Edition). Prentice-Hall Internationals, Inc.

Subaşı, Y. (1998). Fuzzy Control of Brushless Dc Motors. A Thesis Presented to The Graduate School of Natural and Applied Sciences of The Middle East Technical University.

TDA5142T Brushless DC Motor Drive Circuit, 1994, Philips Semiconductors (Datasheet).

The Electric Power Research Institute (Agreement RP3245-03) and The Entergy Corporation. <u>Large Process Industry Motor Drive Performance and Power Quality Analysis</u>.

Wu, M. (1992). <u>Performance Prediction of Permanent Magnet Motor Drives</u>. A Thesis Presented to The Faculty of the Graduate School of the University of New Orleans.

# APPENDIX

## Brushless DC motor drive circuit

### TDA5142T

### FEATURES

- Full-wave commutation without position sensors
- Built-in start-up circuitry
- Six outputs that can drive three external transistor pairs:
  - output current 0.2 A (typ.)
  - low saturation voltage
  - built-in current limiter
- Thermal protection
- Tacho output without extra sensor
- Transconductance amplifier for an external control transistor
- Motor brake facility.

### APPLICATIONS

- High-power applications e.g.:
  - high-end hard disk drives
  - automotive.

### GENERAL DESCRIPTION

The TDA5142T is a bipolar integrated circuit used to drive 3-phase brushless DC motors in full-wave mode. The device is sensorless (saving of 3 hall-sensors) using the back-EMF sensing technique to sense the rotor position. It includes a brake function and 6 pre-drivers able to control FETs or bipolar external transistors. It is ideally suited for high-power applications such as high-end hard disk drives, automotive and other applications.

### QUICK REFERENCE DATA

Measured over full voltage and temperature range.

| SYMBOL | PARAMETER | CONDITIONS | MIN. | TYP. | MAX. | UNIT |
|--------|-----------|-----------|------|------|------|------|
| $V_P$ | supply voltage | note 1 | 4 | – | 18 | V |
| $V_{VMOT}$ | input voltage to the output driver stages | | 3 | – | 18 | V |
| $V_O$ | driver output voltage | $I_O = 100$ mA; lower transistor | – | – | 0.35 | V |
| | | $I_O = 100$ mA; upper transistor | 1.05 | – | – | V |
| $I_{LIM}$ | current limiting | $V_{VMOT} = 14.5$ V; $R_O = 47$ Ω | 150 | 200 | 250 | mA |

### Note

1. An unstabilized supply can be used.

### ORDERING INFORMATION

| TYPE NUMBER | PACKAGE | | | |
|-------------|---------|---|---|---|
| | PINS | PIN POSITION | MATERIAL | CODE |
| TDA5142T | 24 | SOL | plastic | SOT137-1 |

## Brushless DC motor drive circuit

## TDA5142T

**BLOCK DIAGRAM**
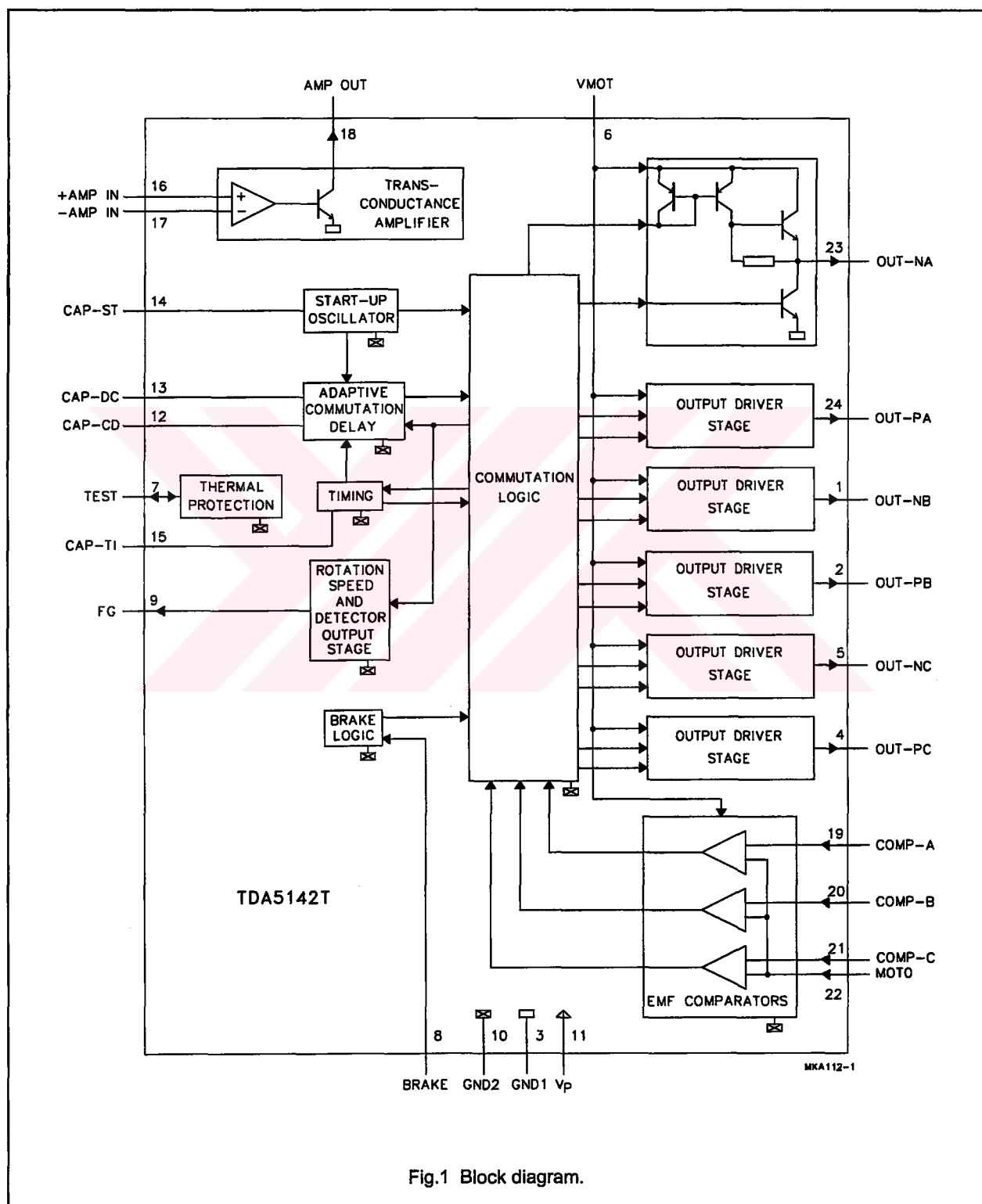


Fig.1  Block diagram.

## Brushless DC motor drive circuit

## TDA5142T

**PINNING**

| SYMBOL | PIN | DESCRIPTION |
|---|---|---|
| OUT-NB | 1 | driver output B for driving the n-channel power FET or power NPN |
| OUT-PB | 2 | driver output B for driving the n-channel power FET or power PNP |
| GND1 | 3 | ground (0 V) motor supply return for output stages |
| OUT-PC | 4 | driver output C for driving the n-channel power FET or power PNP |
| OUT-NC | 5 | driver output C for driving the n-channel power FET or power NPN |
| VMOT | 6 | input voltage for the output driver stages |
| TEST | 7 | test input/output |
| BRAKE | 8 | brake input |
| FG | 9 | frequency generator: output of the rotation speed detector stage |
| GND2 | 10 | ground supply return for control circuits |
| $V_P$ | 11 | supply voltage |
| CAP-CD | 12 | external capacitor connection for adaptive communication delay timing |
| CAP-DC | 13 | external capacitor connection for adaptive communication delay timing copy |
| CAP-ST | 14 | external capacitor connection for start-up oscillator |
| CAP-TI | 15 | external capacitor connection for timing |
| +AMP IN | 16 | non-inverting input of the transconductance amplifier |
| –AMP IN | 17 | inverting input of the transconductance amplifier |
| AMP OUT | 18 | transconductance amplifier output (open collector) |
| COMP-A | 19 | comparator input corresponding to output A |
| COMP-B | 20 | comparator input corresponding to output B |
| COMP-C | 21 | comparator input corresponding to output C |
| MOT0 | 22 | input from the star point of the motor coils |
| OUT-NA | 23 | driver output A for driving the n-channel power FET or power NPN |
| OUT-PA | 24 | driver output A for driving the n-channel power FET or power PNP |

# Brushless DC motor drive circuit

# TDA5142T



Fig.2 Pin configuration.
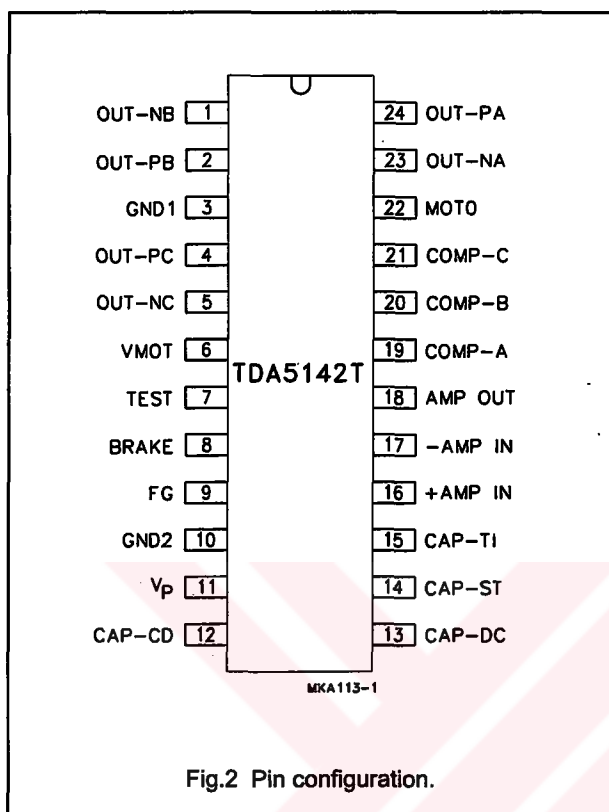
## FUNCTIONAL DESCRIPTION

The TDA5142T offers a sensorless three phase motor drive function. It is unique in its combination of sensorless motor drive and full-wave drive. The TDA5142T offers protected outputs capable of driving external power FETs or bipolar power transistors. It can easily be adapted for different motors and applications. The TDA5142T offers the following features:

- Sensorless commutation by using the motor EMF.
- Built-in start-up circuit.
- Optimum commutation, independent of motor type or motor loading.
- Six output drivers.
- Maximum output current 0.25 A.
- Outputs protected by current limiting and thermal protection.
- Low current consumption.
- Accurate frequency generator (FG) by using the motor EMF.
- Brake function.
- Uncommitted operational transconductance amplifier (OTA), with a high output current, for use as a control amplifier or as a level shifter in a Switched Mode Power Supply (SMPS) drive.

## LIMITING VALUES

In accordance with the Absolute Maximum Rating System (IEC 134).

| SYMBOL | PARAMETER | CONDITIONS | MIN. | MAX. | UNIT |
|---|---|---|---|---|---|
| $V_P$ | supply voltage | | 4 | 18 | V |
| $V_I$ | input voltage; all pins except VMOT | $V_I < 18$ V | −0.3 | $V_P + 0.5$ | V |
| $V_{VMOT}$ | VMOT input voltage | | 3 | 18 | V |
| $V_O$ | output voltage | | | | |
| | FG | | GND | $V_P$ | V |
| | AMP OUT | | − | 18 | V |
| | OUT-NA, OUT-NB and OUT-NC | | − | $V_{VMOT} - 0.9$ | V |
| | OUT-PA, OUT-PB and OUT-PC | | 0.2 | − | V |
| $V_I$ | input voltage CAP-ST, CAP-TI, CAP-CD and CAP-DC | | − | 2.5 | V |
| $T_{stg}$ | storage temperature | | −55 | +150 | °C |
| $T_{amb}$ | operating ambient temperature | | 0 | +70 | °C |
| $P_{tot}$ | total power dissipation | see Fig.3 | − | − | W |
| $V_{es}$ | electrostatic handling | see Chapter "Handling" | − | 500 | V |

## Brushless DC motor drive circuit

## TDA5142T


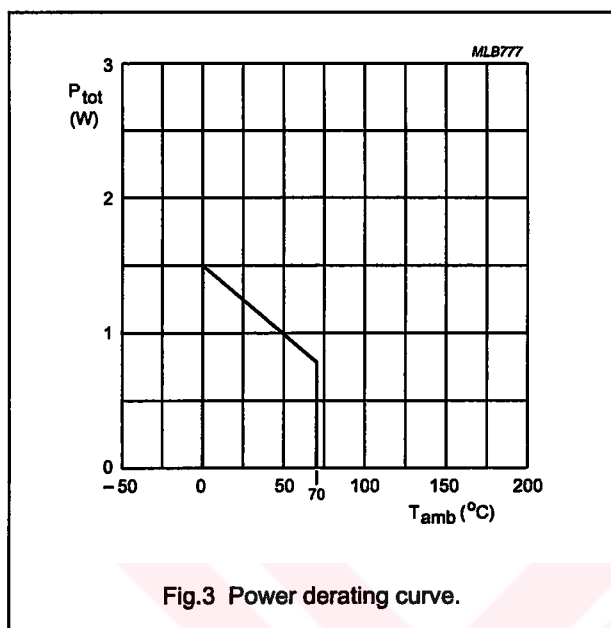
Fig.3 Power derating curve.

### HANDLING

Every pin withstands the ESD test according to *"MIL-STD-883C class 2"*. Method 3015 (HBM 1500 Ω, 100 pF) 3 pulses + and 3 pulses − on each pin referenced to ground.

### CHARACTERISTICS

$V_P$ = 14.5 V; $T_{amb}$ = 25 °C; unless otherwise specified.

| SYMBOL | PARAMETER | CONDITIONS | MIN. | TYP. | MAX. | UNIT |
|--------|-----------|------------|------|------|------|------|
| **Supply** | | | | | | |
| $V_P$ | supply voltage | note 1 | 4 | – | 18 | V |
| $I_P$ | supply current | note 2 | – | 5.2 | 6.25 | mA |
| $V_{VMOT}$ | input voltage to the output driver stages | see Fig.1 | 3 | – | 18 | V |
| **Thermal protection** | | | | | | |
| $T_{SD}$ | local temperature at temperature sensor causing shut-down | | 130 | 140 | 150 | °C |
| $\Delta T$ | reduction in temperature before switch-on | after shut-down | – | $T_{SD} - 30$ | – | K |
| **COMP-A, COMP-B, COMP-C and MOT0** | | | | | | |
| $V_I$ | input voltage | | –0.5 | – | $V_{VMOT}$ | V |
| $I_I$ | input bias current | 0.5 V < $V_I$ < $V_{VMOT}$ − 1.5 V | –10 | – | 0 | μA |
| $V_{CSW}$ | comparator switching level | note 3 | ±20 | ±25 | ±30 | mV |
| $\Delta V_{CSW}$ | variation in comparator switching levels | | –3 | 0 | +3 | mV |
| $V_{hys}$ | comparator input hysteresis | | – | 75 | – | μV |

## Brushless DC motor drive circuit

## TDA5142T

| SYMBOL | PARAMETER | CONDITIONS | MIN. | TYP. | MAX. | UNIT |
|---|---|---|---|---|---|---|
| **OUT-NA, OUT-NB, OUT-NC, OUT-PA, OUT-PB and OUT-PC** | | | | | | |
| $V_{O-n}$ | n-channel driver output voltage | upper transistor; $I_O = -100$ mA | −1.05 | – | – | V |
| | | lower transistor; $I_O = 10$ mA | – | – | 0.35 | V |
| $V_{O-p}$ | p-channel driver output voltage | upper transistor; $I_O = -10$ mA | −1.05 | – | – | V |
| | | lower transistor; $I_O = 100$ mA | – | – | 0.35 | V |
| $\Delta V_{OL}$ | variation in saturation voltage between lower transistors | $I_O = 100$ mA | – | – | 180 | mV |
| $\Delta V_{OH}$ | variation in saturation voltage between upper transistors | $I_O = -100$ mA | – | – | 180 | mV |
| $I_{LIM}$ | current limiting | $V_{VMOT} = 14.5$ V; $R_O = 47\ \Omega$ | 150 | 200 | 250 | mA |
| **+AMP IN and −AMP IN** | | | | | | |
| $V_I$ | input voltage | | −0.3 | – | $V_P - 1.7$ | V |
| | differential mode voltage without 'latch-up' | | – | – | $\pm V_P$ | V |
| $I_b$ | input bias current | | – | – | 650 | nA |
| $C_I$ | input capacitance | | – | 4 | – | pF |
| $V_{offset}$ | input offset voltage | | – | – | 10 | mV |
| **AMP OUT (open collector)** | | | | | | |
| $I_{sink}$ | output sink current | | 40 | – | – | mA |
| $V_{sat}$ | saturation voltage | $I_I = 40$ mA | – | 1.5 | 2.1 | V |
| $V_O$ | output voltage | | −0.5 | – | +18 | V |
| SR | slew rate | $R_L = 330\ \Omega$; $C_L = 50$ pF | 40 | – | – | mA/µs |
| $G_{tr}$ | transfer gain | | 0.3 | – | – | S |
| **BRAKE** | | | | | | |
| $V_{BM}$ | brake-mode voltage | enable brake mode; $4\ V < V_P < 18\ V$ | | – | 2.3 | V |
| | | normal mode; $4\ V < V_P < 18\ V$ | 2.7 | – | | V |
| $I_I$ | input current | brake mode | – | −20 | −30 | µA |
| | | normal mode | – | 0 | 20 | µA |

## Brushless DC motor drive circuit

## TDA5142T

| SYMBOL | PARAMETER | CONDITIONS | MIN. | TYP. | MAX. | UNIT |
|---|---|---|---|---|---|---|
| **FG (push-pull)** | | | | | | |
| $V_{OL}$ | LOW level output voltage | $I_O = 1.6$ mA | – | – | 0.4 | V |
| $V_{OH}$ | HIGH level output voltage | $I_O = -60$ μA | | $V_P - 0.3$ | – | V |
| $t_{THL}$ | HIGH-to-LOW transition time | $C_L = 50$ pF; $R_L = 10$ kΩ | – | 0.5 | – | μs |
| | ratio of FG frequency and commutation frequency | | – | 1 | – | |
| **CAP-ST** | | | | | | |
| $I_{sink}$ | output sink current | | 1.5 | 2.0 | 2.5 | μA |
| $I_{source}$ | output source current | | –2.5 | –2.0 | –1.5 | μA |
| $V_{SWL}$ | LOW level switching voltage | | – | 0.20 | – | V |
| $V_{SWH}$ | HIGH level switching voltage | | – | 2.20 | – | V |
| **CAP-TI** | | | | | | |
| $I_{sink}$ | output sink current | | – | 28 | – | μA |
| $I_{source}$ | output source current | $0.2$ V $< V_{CAP-TI} < 0.3$ V | – | –57 | – | μA |
| | | $0.3$ V $< V_{CAP-TI} < 2.2$ V | – | –5 | – | μA |
| $V_{SWL}$ | LOW level switching voltage | | – | 50 | – | mV |
| $V_{SWM}$ | MIDDLE level switching voltage | | – | 0.30 | – | V |
| $V_{SWH}$ | HIGH level switching voltage | | – | 2.20 | – | V |
| **CAP-CD** | | | | | | |
| $I_{sink}$ | output sink current | | 10.6 | 16.2 | 22 | μA |
| $I_{source}$ | output source current | | –5.3 | –8.1 | –11 | μA |
| $I_{sink}/I_{source}$ | ratio of sink to source current | | 1.85 | 2.05 | 2.25 | |
| $V_{IL}$ | LOW level input voltage | | 850 | 875 | 900 | mV |
| $V_{IH}$ | HIGH level input voltage | | 2.3 | – | 2.5 | V |
| **CAP-DC** | | | | | | |
| $I_{sink}$ | output sink current | | 10.1 | 15.5 | 20.9 | μA |
| $I_{source}$ | output source current | | –20.9 | –15.5 | –10.1 | μA |
| $I_{sink}/I_{source}$ | ratio of sink to source current | | 0.9 | 1.025 | 1.15 | |
| $V_{IL}$ | LOW level input voltage | | 850 | 875 | 900 | mV |
| $V_{IH}$ | HIGH level input voltage | | 2.3 | – | 2.5 | V |

**Notes**

1. An unstabilized supply can be used.

2. $V_{VMOT} = V_P$, all other inputs at 0 V; all outputs at $V_P$; $I_O = 0$ mA.

3. Switching levels with respect to driver outputs OUT-NA, OUT-NB, OUT-NC, OUT-PA, OUT-PB and OUT-PC.

## Brushless DC motor drive circuit
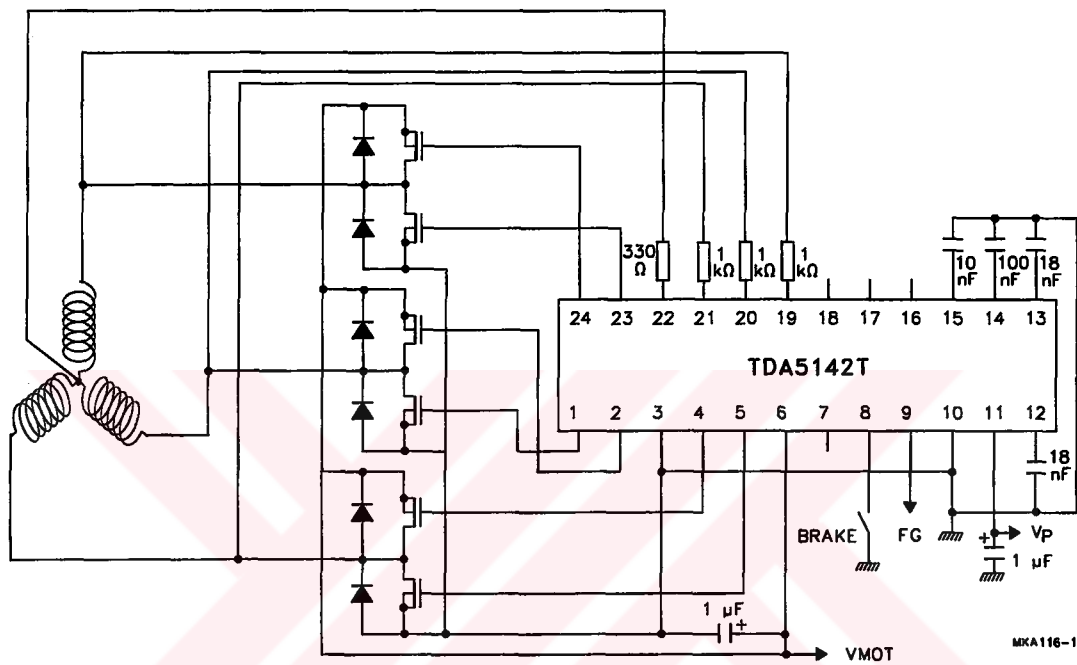
## TDA5142T

**APPLICATION INFORMATION**
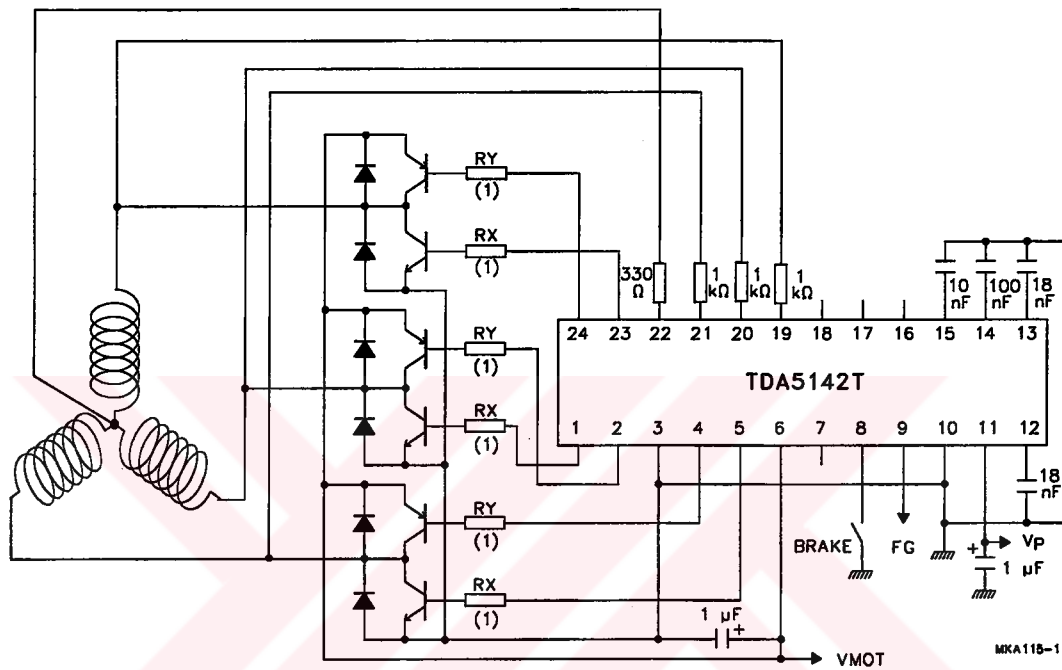


(1)  RX = RY > 8 (VMOT − 1.5)

Fig.4   Application diagram without use of the operational transconductance amplifier (OTA) with bipolar
power transistors.

## Brushless DC motor drive circuit

## TDA5142T



Fig.5    Application diagram without use of the operational transconductance amplifier (OTA)
with MOSFETs.